MICROSTRUCTURAL AND MECHANICAL CHARACTERIZATION OF ZEOLITE ENHANCED WELLBORE CEMENT FOR PLUGGING AND ABANDONMENT

By

SAI VAMSI KRISHNA VISSA

Bachelor of Science in Biosciences (Honors)

Sri Sathya Sai Institute of Higher Learning

Bangalore, Karnataka, India

2014

Master of Science in Nanoscience and Nanotechnology

Sri Sathya Sai Institute of Higher Learning

Puttaparthi, Andhra Pradesh, India

2016

Submitted to the Faculty of the
Graduate College of the
Oklahoma State University
in partial fulfillment of
the requirements for
the Degree of
MASTER OF SCIENCE
December, 2021

MICROSTRUCTURAL AND MECHANICAL CHARACTERIZATION OF ZEOLITE ENHANCED WELLBORE CEMENT FOR PLUGGING AND ABANDONMENT

Thesis Approved:

Dr.Mileva Radonjic

Thesis Adviser

Dr.Tyler ley

Dr.Mohammed Al Dushaishi

Dr.Ozgur Capraz

ACKNOWLEDGEMENTS

First and foremost, I would like to thank my advisor Dr. M. Radonjic for giving me this wonderful opportunity to undertake this challenging endeavor. It had been a great learning experience during the course of my program. I thank her for the constant support and guidance, this dissertation would not have been possible. The NAS-GRP is gratefully acknowledged for funding this work. Thanks are due to the Dr. G. Trabits, Trabits group for providing us with zeolite samples and also the commercial zeolite cement formulation. We thank Dr. L. Leotaud from NexTier oilfield solution.inc for help with developing the 16PPG zeolite cement slurries. Special thanks to Mr. B. Johnson and Ms. L. Whitworth from the Oklahoma State Microscopy Centre whose support had been indispensable. Sincere thanks to Mr. E. Cline from Chesapeake Energy for their support in acquiring the UCS data of the cement cores. I sincerely thank Dr. A. Bunger, and Y. Lu for providing us with important data acquired from the Triaxial test set-up at the University of Pittsburgh. I would like to extend my sincere Thanks to Dr. D. Crandall at National Energy Technology Laboratory (NETL), for acquiring high resolution CT images of the various cement formulations prior and after triaxial testing. I thank all the members of our NAS-GRP project for their valuable inputs in the several progress meetings we had over the past two years. I am grateful to Dr. T. Ley, Dr. M. Al Dushaishi, Dr. O. Capraz for kindly agreeing to be a part of my research advisory committee and providing me with valuable insights from their immense experience. Last but not the least we would like to thank our team members for their continuous support during this work: C. Massion, A. Katende, C. Ferguson, Dr. M. Achang, Dr. G. Luo.

Acknowledgements reflect the views of the author and are not endorsed by committee members or Oklahoma State University.

Name: SAI VAMSI KRISHNA VISSA

Date of Degree: DECEMBER, 2021

Title of Study: MICROSTRUCTURAL AND MECHANICAL CHARACTERIZATION OF ZEOLITE ENHANCED WELLBORE CEMENT FOR PLUGGING AND ABANDONMENT

Major Field: PETROLEUM ENGINEERING

Abstract: plugging and abandonment (P&A) of wellbores have not seen the same amount of development that is seen in wellbore construction and exploration. Off shore wellbores face various challenges in the case of P&A as they need to maintain complete zonal isolation. With almost 281 kilotons of methane released every year from 3.2 million abandoned wells, it is crucial to reduce the leakage of hydrocarbons from a global warming perspective. In order to make these plugs more robust, additives are needed to improve the quality of the cement used for these purposes. Zeolite, had been studied as an additive to cement showing improvement in cement properties which are discussed in the coming chapters. The addition of zeolites had shown an improvement in various cement properties as observed in the literature. A zeolite ferrierite had been adapted from the geothermal application. 5% by weight of cement ferrierite added cores had shown improvement of properties like UCS by about 41% in comparison to neat Class-H cement based cores. It had also shown an improvement in triaxial strength tests with a 68.8MPa peak stress shown for 5% ferrierite compared to 62.9MPa for neat Class-H cement. petrophysical property improvement had been seen for 5% ferrierite addition as it had the lowest permeability of 13.54μD which is lower than that of neat Class-H cement (49.53 μD). The results of 15% as well as 30% additions had been reported in this work and the overall performance makes it a contender for our application in P&A.

TABLE OF CONTENTS

Chapter Page

LIST OF TABLES

Table Page

LIST OF FIGURES

Figure Page

Figure Page

CHAPTER I

INTRODUCTION

1.1 Wellbore cementing – Challenges:

Many oil and gas wells were constructed for ages to meet the growing energy demand. Cement was extensively used for constructing these oil and gas wells. These wells are abandoned when productivity is not economically viable anymore. Permanent plugging is required to prevent leakage of residual hydrocarbons from these wells into the environment damaging the ecosystem. According to the United States Energy information administration (EIA), the number of producing wells reduced from 1,029,000 in 2014 to 969,140 in 2019[1]. Bureau of Ocean Energy Management (BOEM) estimates at least 3000 wells and 650 platforms that are not in use and in need of plugging and abandonment in the Gulf of Mexico (GoM) alone†.

Plugging and abandonment of these unproductive wells had been in practice for several decades and had seen notable advances in the cement designs. Given the challenges of sub-surface wells off shore, including High temperature and High pressure (HTHP) conditions, and reactive chemical conditions,[2-8] the cement formulations meant for this purpose needs to be more durable for wellbore construction and later stages of well completion like plugging and abandonment[5, 8-11]. The inspiration comes from natural cap-rocks which had survived these adverse conditions for millions of years. The aim of this research is to engineer cement-based composite similar to geological cap-rocks. The properties of cement ultimately depend on the reaction of cement with water known as hydration[12-17].

Reinforced cement concrete is a very standard and highly advanced material used in many land constructions, but wellbore construction demands pumping of cement over very long distances sometimes thousands of feet downhole for which concrete is not the right material as it faces challenges like segregation [18-21] and sometimes the coarse aggregates disrupt the flow. To avoid these hindrances, cement is pumped as a paste for wellbore construction operations to keep cement slurry stable throughout the pumping process. Chemical admixtures as well as nano and micro additive materials [22-26] can be used with the cement slurry to control the rheology while pumping the mixtures. This study does not include the rheological property study as it is a property that can be controlled on-site using various chemical and mineral admixtures. Many insights have been acquired from concrete [19, 27-36], used for land constructions predominantly. Despite the similarity in cement chemistry, special care needs to be taken for preparing these formulations to use in offshore wellbore construction as well as in plugging and abandonment [37-42].

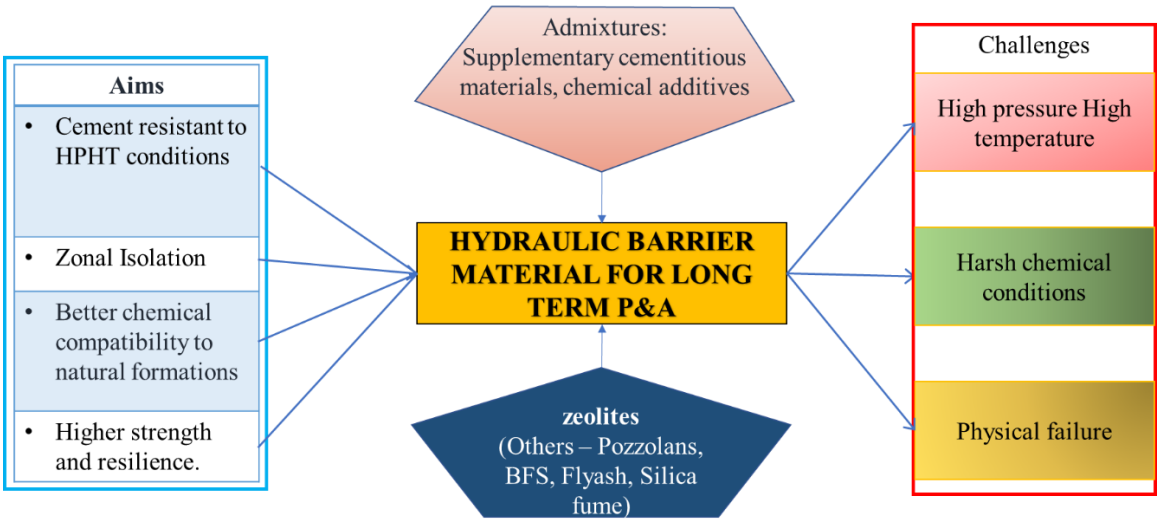

Fig-1.1. Challenges in the usage of cement for sub-surface conditions, additives and the aims of this research. The aim of the formulation to be made is to have very low porosity and permeability (Petrophysical properties) to ensure the integrity of the wellbore, to prevent leakage of hydrocarbons, and have higher resistance to HTHP conditions and harsh

downhole chemical conditions (Presence of corrosive/acidic conditions which have a deteriorating effect on cement [43, 44]). The cement also needs to have more strength and resilience which include elastic over brittle nature of hydrated cement pastes to avoid failures and also the ability to self-heal in case of a failure[45-48].

Aforementioned adverse conditions have a deteriorating effect on cement and it needs to be resistant to these conditions to avoid any hydrocarbon leakage. The durability of the cement formulations is the biggest concern for the long-term sealing of wellbores. In figure-1 above, the schematic of challenges and proposed solutions for cement enhancement, are seen. Due to these adverse conditions, deterioration and failure of cement occurs and leakage pathways would be created [49-51]. Various leakage pathways could occur due to phenomena like:

1) Shear failure: Results due to uneven or pointed pressure increase on the cement sheath.
2) Inner debonding: This is the debonding that happens between the cement sheath and the metal casing. This could create a leakage pathway.
3) Outer de-bonding: This is the debonding that happens between the cement sheath and the formation creating a leakage pathway.
4) Radial cracking: This could be observed in cement plugs where the fractures could appear in a radial pattern [52]
5) Disking: Occurs either in the cement sheath or the cement plug, with disk-like fractures which disrupt the zonal isolation. The leakage pathways created due to these types of fractures might result in debonding in later stages.
6) Other failures: Other failures include degradation of cement sheath or plug due to phenomena like casing corrosion, abnormal pH conditions, high temperatures and pressures etc. Contamination from drilling mud is also possible during the cementing jobs and could pose a threat to the integrity of the cement sheath. Chemical attacks like sulfate

attack or other ionic attacks could cause degradation or failure of cement.

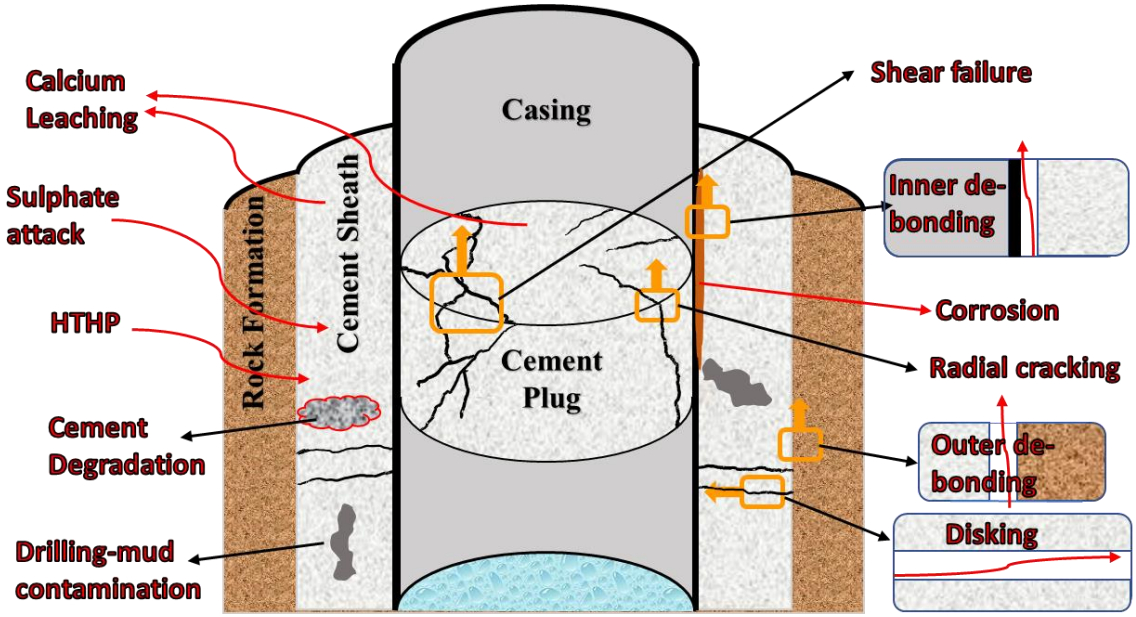

Fig-1.2. The various leakage pathways [51, 53] that could be observed in a wellbore cement plug. While inner de-bonding is the leakage pathway created by the de-bonding occurring between the cement sheath/plug and the casing, outer de-bonding occurs between the cement sheath and rock formation of the reservoir into which the well was drilled. Disking could occur in the cement sheath around the casing. These are basically disk-like fractures spreading continuously around the casing. Shear failure and Radial cracking could take place in the cement plug itself causing leakage pathways for hydrocarbons.

In order to tackle these challenges, research had been directed towards making more robust cement slurry designs by adding various admixtures and additives to cement. Also, different types of cement are preferred for different applications. The following literature review aims to give a basic introduction to the most common cement and concrete admixtures mainly concentrating on mineral admixtures which give cement its long-term properties for both land structures and wellbores. This is followed by preliminary results obtained during the course of this research, discussion of those results, and future plan of action.

1.2. Objectives:

The objectives of current research are to develop a cement design with an additive material of choice and test the resultant design for chemical, mechanical and petrophysical properties. The first part of this research includes a literature survey to choose the ideal additive material. The material would be studied independently to get insights into its chemical properties. The material is then tested with cement. Formulations would be made with different proportions of the additive materials by weight of cement (BWoC) and they would be tested for the above-mentioned properties using the various characterization tools that would be explained in detail in the methodology section. The final objective is to interpret the results of the characterization techniques and support the usage of material in cement for plugging and abandonment, recommending our formulations.

1.3. Research aims:

The long term goal of this research is to develop cement designs that can sustain for hundreds of years downhole by being resistant to chemical attacks, and maintaining structural integrity. The resultant plugs should be able to prevent any leakage of hydrocarbons into the surrounding environment. In order to do so, the additive materials that need to be added are to be tested and the resultant cement cores are characterized for physical, chemical, morphological, and petrochemical properties. This work is going to highlight the initial test results, discuss the outcome of those tests and conclude with the key observations, explaining the mechanism to support the hypothesis based on the results. This will also include the future recommendations for this work to be completed in a more detailed procedure. This research had been part of a NASEM funded project and will be reported to the funding agency as required. By the end of this work, we would have an insight into the mechanism justifying our hypothesis based on the results and provide recommendations for further research.

CHAPTER II

REVIEW OF LITERATURE

2.0. Research into cement admixtures:

Cement is a broadly used material for many construction purposes and it is the main material used for wellbore construction. However, cement as a material on its own has got several challenges like brittleness, low resistance to chemical attacks and high temperatures and pressures. Based on the application for which cement needs to be used, extensive research had been done to classify materials that can be used to enhance the properties of cement accordingly. Many cement admixtures had been in use for several decades and the major materials that had been used for this purpose are described below. Cement admixtures are of 4 broad classes based on their effect on cement according to Mindess S.et al. (2003)[54]:

1. Air entraining agents (ASTM C260): These work by entrapping microscopic air bubbles during the hardening of the cement. This improves workability as well as reduces bleeding and segregation of cement while hydrating. This is helps improve the freeze-thaw resistance [55].

2. Chemical admixtures (ASTM C494): These are admixtures that are usually water-soluble and in addition to cement disperse easily in the wet mixture. These control the setting properties of cement by retardation or acceleration, as well as the water requirement for the slurry. They are divided into different types based on their function

3. Mineral admixtures (STP169A-EB): These are usually particles of natural or artificial minerals which are added to cement as pulverized solids. These improve the durability and strength properties of cements upon setting. Some supplementary cementitious materials like slag and pozzolans fall under this category [56]

4. Miscellaneous admixtures are all those which do not fall under the aforementioned classes. They are developed for achieving specific properties in cement and affect the cement properties by more than one means.

While air-entraining agents and chemical admixtures are essential for the workability and initial properties of the cement slurry, current research is directed towards the long-term effects of mineral admixtures on hydrated cement properties. The durability and strength of the cement for an extended period are the focus as researchers aim to achieve a permanent solution without the need for frequent repairs and remedial cementing. This project explores cement as a material mainly for plugging and abandonment purposes rather than the other well structures which means that this cement formulation must have very low porosity and permeability without affecting the strength properties. This makes it stable and avoids leakage of hydrocarbons through various pathways like fractures and pore spaces. Leakage pathways would be created as mentioned in the introduction due to adverse conditions observed downhole. Many mineral admixtures had been studied over the period of several years [25, 57-60] as admixtures in cement improve the strength and durability of the resultant structures.

2.1. Research in Mineral admixtures:

Many mineral admixtures had been studied as additives for cement over several decades both in land constructions as well as for wellbore constructions. Cement faces common issues in both the cases and research from the construction industry is adapted to wellbore construction. Literature survey had been performed to discuss the advantages and disadvantages of mineral admixtures

providing valuable insights to choose the ideal additive material. At the end of this section, the knowledge gaps would be discussed before summarizing the advantages and disadvantages of the materials studied as SCMs. Once the knowledge gaps are identified for the material of choice, further research is conducted to understand and fill the gaps.

2.2. Pozzolana:

Pozzolana/pozzolans are a class consisting of an extensive range of siliceous materials which occur naturally as volcanic incoherent pozzolans, sedimentary or as diagenized materials formed due to chemical processes that take place at hot springs or volcanic activity. They are also present as pyroclastic and clastic rocks in nature. They possess low cementitious properties, but when reacted. with lime and water, they produce hydraulic materials rich in C-S-H which is a major product in the initial reaction period of cement hydration. This leads to increased strength in the resultant cement as well as reduced porosity and permeability compared to plain Portland cement. They have the glass phase which is predominantly silica with smaller amounts of alumina and Fe2O4, which is the active phase and takes part in hydration.

2.2.1. (a) Advantages of pozzolana:

These are the materials that are often referred to as natural supplementary cementitious materials. However, other materials which show pozzolanic activity are also used as supplementary cementitious materials which include burnt or calcined clays and other thermally activated materials. They show an enhancement in the cement properties by means of pozzolanic reaction which is defined as the reaction of the active phases of lime and pozzolanic materials in the presence of water. This reaction depends on various parameters including the pozzolan-lime ratio, the nature of active phases present, and the SiO_2 content in the mixture. The pozzolanic reaction does not directly affect the cement hydration, but it enhances overall strength [61] and durability by the following means:

a. Forming more reactive phases acting as active sites for hydration to take place.

b. SiO_2 and Al_2O_3 in the pozzolanic glasses react with lime to form an unreactive phase which act as fillers in the resultant cement, decreasing the porosity and permeability which adds to the ultimate durability.

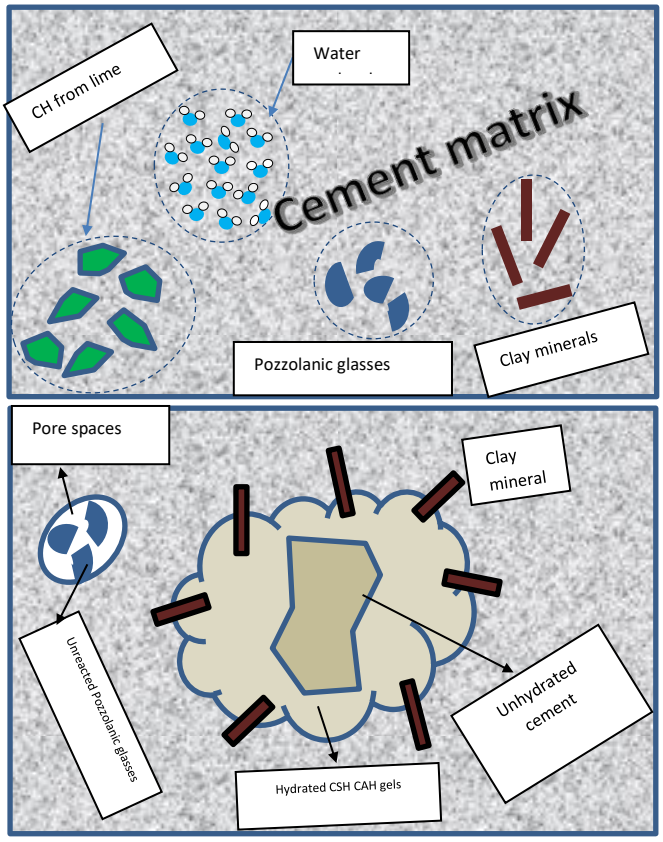

Fig-2.1. A basic schematic of the pozzolanic reaction with clay minerals acting as substrates for hydration as well as reacting with lime and cement minerals to form CSH and CAH gels. The unreacted pozzolanic glasses like Al_2O_3 and SiO_2 occupy the pore spaces acting as fillers. This could be the basic underlying mechanism for most of the cement additives and helps us hypothesize mechanism for other additives.

However, natural pozzolana addition did not improve the compressive strength properties of cement substantially. They required thermal activation in some cases to get the best property enhancement. It was also noted that as days progressed, the increase in pozzolan content added to the strength improvement mainly by filler effect rather than by active pozzolanic reaction [62]. Calcium hydroxide, or CH, is one of the Portland cement products that takes part in the pozzolanic reaction. This was determined by many researchers in previous studies where they obtained a direct correlation between the CH content and the content of pozzolans like metakaolins, etc.[63] added to the cement mixtures. Wild et al. (1996,2001)[64, 65] stated that metakaolin adds to the cement

properties in three ways: vis. filler effect, acceleration of ordinary Portland cement (OPC) hydration, and the pozzolanic reaction itself [66]. Filler effect is observed due to the micro/nano-particles filling up the pore spaces giving additional strength to the material. Pozzolanic reaction and hydration are two native cement reactions that result in formation of stronger hydrated phases an enhancement of this phase formation by any means would inherently improve the strength of the resultant material.

The pozzolanic reaction is also seen in other classes of additives like fly ash and silica fume [67]. Despite a higher degree of pozzolanic reaction, clinoptilolite addition showed a reduced 28-day strength in the concrete owing to the pore spaces present in the zeolitic cement [68] in comparison to its silica fume (SF) and fly ash (FA) counterparts. Clinoptilolite addition, however, resulted in a more stable concrete in terms of permeability and ion transport properties [69]. It had a very high resistance to ionic attacks as compared to the silica fume and fly ash, as those materials show strength enhancement mainly by filler effect and other physical effects more than pozzolanic reaction. In other words, the degree of pozzolanic reaction affects the chemical stability of resultant cement but does not directly affect the strength and other physical properties.

2.2.2. Limitations of pozzolana:

The pozzolanic reaction depends on the ready availability of aluminates and silicates for the formation of CAH or CSH. Most naturally occurring pozzolans do not have them readily available but as a part of the material, which makes it tougher for the CH to react. So, direct addition of pozzolans does not show immediate effect but takes time for the release of aluminates or silicates and hence shows enhancement in later properties than the initial hydration. To get the best out of pozzolans, it is required to use chemically or thermally activated pozzolans which increases the availability of aluminates or silicates for the hydration reaction. Most often than not, the pozzolans act as fillers instead of actively taking part in the hydration reaction.

2.3. Slag or Blast furnace slag:

Blast furnace slag (BFS) or simply slag is the calcium silicate–based product removed from the top of molten iron during its extraction from ore in a blast furnace; usually rapidly cooled to a glassy state and ground for use in construction materials. GGBFS or ground granulated blast furnace slag is the commonly used form these days in the cement industry. These types of cement are promising given their late strength enhancement, but conclusive results had not been shown regarding the porosity and permeability as those properties depend on the speed of the hydration reaction which is defined by several other factors including Alkaline additions, the temperature of the reaction etc.

2.3.1. Advantages of Blast furnace slag:

This is another supplementary cementitious material of interest. It is shown to have better properties on addition to cement on exposure of cement to higher temperatures. In general, loss of strength is observed for ordinary cements at elevated temperatures as it affects the microstructural properties, permeability and other physical properties of cement. Despite the initial decrease of strength, and an overall decrease of the 28-day strength at room temperature, the slag cement is shown to have better compressive strengths at more than 100ºC and it is best between 200-300ºC [70]. This could make the resultant cement more stable at elevated temperatures and useful for a wide range of applications like in geothermal wells, oil well cementing [71] or even nuclear plants. While slag cements had been used for a while now with up to 35% granulated BFS replacements of cement by weight, the additions of cement kiln dust and silica fume in varying proportions to the slag cement was shown to influence the compressive strength. The 28-day compressive strength was noted to increase from 60.1MPa in normal slag cement (control) to 71.6MPa [72] in a mixture where 10% cement kiln dust and 5% silica fume were used to replace slag cement by weight. Slag additions have shown fluid loss, free fluid and compressive strength properties comparable and even better

than the ordinary Portland cement in some cases [71]. Alkali activated slag-fly ash blends were shown to positively affect the mechanical performance of cement.

To have a better understanding of the slag hydration mechanism, Wang S.D., Scrivener K.L.et al (1995) studied the products of slag on alkali activation using alkaline solutions of sodium hydroxide and water glass ($NaO_2.SiO_2$) solutions. They have noticed that irrespective of the activator, the major hydration product was C-S-H which was the same as in cement but had a lower Ca/Si ratio [73]. Similar work was done by Luke K. et al., (1987) [74]

Slag was also shown to have better reactivity when an alkaline activator, like sodium silicate was used. The cements made by varying amounts of slag and fly ash proportions by alkali activation were studied by autoclaving them at elevated temperatures of 100-300ºC and exposing them to strong acids like H_2SO_4 with CO_2 dissolved in it at around 90ºC and the weight loss was studied by Sugama T. et al (2005) to check the acid resistance [75].

A review was published by Ozbay et al E. (2016) which was a very recent account where the advantages of using granulated blast furnace slag were recorded. [76]. The chemical properties of slag however, depend on the basicity of the slag which varies based on the quantities of each of the components present in the slag which are CaO, SiO_2, MgO and alumina.

Palou M.T. et al (2016) had studied the synergistic effects of the quaternary mixtures of BFS, silica fume and metakaolin and had noted that the compressive strength values for 7 days and 28 days had been highest for the 5%BFS, 15%SF and 5%MK replacement in cement. [77]. Deboucha W. Et al (2016) [78] had studied the properties of cement on individual additions of BFS and Natural Pozzolans. He had noted that for the required water binder ratios of those cement slurries for optimum hydration, natural pozzolan mixtures of all the mix ratios that he had studied, had shown a lower compressive strength compared to the cements in which BFS was added. This shows an apparent advantage of adding BFS over adding natural pozzolans alone.

2.3.2. Limitations of Blast furnace slag:

Since blast furnace slag is an industrial waste, the control on the purity of this additive is very limited. As the distribution of the phases is random, the properties of one batch may differ from another batch of additive. Since slag predominantly consists of oxides, it does not directly take part in the hydration reaction but acts as a filler in most cases. Activation of slags with alkali helped in improving the hydration properties, by which the slag actively participates in the hydration reaction forming cement phases. The downside is that activation of slag is an additional process that takes time and money increasing the costs of production and as a result, the cost of the raw material that is required as the additive in cement would not make it the ideal choice. Hence, BFS despite its advantages is not a widely popular alternative as an additive unless the application requires a specific cement property that can be achieved using BFS alone.

2.4. Fly ash:

Also known as pulverized fuel ash (PFA), is a by-product of coal electrical generators. The waste that is produced by the burning of coal is predominantly aluminosilicates which is glassy in nature and the particles have a spherical shape. The structural differences in this occur based on the CaO content in the fly ash which is dependent on the type of coal that had been used as the fuel. The calcium content also influences the acceleration or retardation of the hydration reaction. It gives the flexibility to use it as SCM when acceleration or retardation of the cement setting.

2.4.1. Advantages of fly ash:

It is another well-known pozzolanic material used as a cement admixture since the early 1930s and was introduced in the US in the late 1970s [33]. Fly ash or pulverized fuel ash (PFA) is obtained from the burning of pulverized coal and is classified into Class F and Class C PFA based on the calcium content. Earlier studies had shown that PFA has a notable effect on the strength[79],

permeability and ion transport characteristics of cement. Bijen J. et al., (1996) [80] mentions that the initial porosity was high for PFA, but it reduced as the hydration progressed.

The fineness of the fly ash particles was also shown to have a varying effect on the strength properties of the cement. P.Chindaprasirt Et al (2005) [81] studied the difference between the properties of cement with original fly ash versus classified fly ash. While the original fly ash (OFA) has larger fly ash particles with sizes of up to 19.1μm, classified fly ash (CFA) has an average particle size distribution of 6.4μm. These studies showed that while varied OFA additions showed a decrease in the strength and increase in the porosity values compared to the normal cement samples, CFA additions had a positive effect on the strength which showed a notable increase compared to plain Portland cement samples. The finer CFA also had shown decreased total and capillary porosity values compared to those observed in OFA added to the cements.

The hydration properties of FA were studied in comparison to silica fume by B.W. Langan Et al (2002) [82]. The study of the rate of hydration in this case, shows that the addition of fly ash retards the rate of hydration mainly in the dormant and the acceleration periods. They had also studied the hydration properties of adding both SF and FA, in which case there was an overall decrease in the heat of hydration and a retardation in the rate of hydration.

2.4.2. Limitations of fly ash:

Since these do not have any effect on the hydration reaction, they do not improve the initial strength properties of the cements. However, due to the filler effect, they later occupy the pore spaces and hence improve the petrophysical properties like porosity and permeability. They do not improve the chemical properties of cement in a direct manner by taking part in the hydration, but prevent chemical attacks by effectively blocking pore spaces and as a result reducing permeability to harsh chemicals from the environment and ultimately providing the necessary resistance from chemical attacks.

2.5. Silica fume:

This is predominantly SiO_2 (up to 90%). Fe_2O_4 is a major secondary oxide with all other oxides less than 1% of the whole composition. Silica fume or condensed silica fume is formed by the condensation of silicon monoxide, which is oxidized to form silicon dioxide or silica, giving rise to highly reactive spherical aggregates which show hydraulic properties. This is a by-product of the silicon manufacturing industry. They are mostly used as a replacement for cement, but in some cases, the addition of silica fume as supplementary cementitious material had shown positive effect on the properties of cement including reduced porosity and permeability, as well as increased strength. This was introduced into cement as a rich source of silica which is one of the building blocks of cement in formation of the hydrated cement phases.

2.5.1. Advantages of silica fume:

This is another SCM that had been widely used in the cement industry. The property enhancement of cement with SF was tested for the first time in the early 1950s. Silica fume was shown to induce a substantial increase in compressive strength [83] and also showed better durability properties like low permeability and resistance to ionic attacks. Silica fume also shows pozzolanic activity, but it mainly reduces the porosity by the micro filler effect in the initial stages. Silica Fume particles were shown to produce a layer rich in silica and poor in calcium on rapid dissolution in CH solution which could act as a substrate for the hydration reaction and subsequently formation of C-S-H crystals [82]. The addition of silica fume to the cement mixtures results in the formation of SF layers on the cement particle surfaces and also adsorb water. This reduces the amount of water available for hydration and in turn retards the hydration process. But once the calcium ions start passing through the collected water, pozzolanic reaction kicks in resulting in the formation of C-S-H which ultimately results in the betterment of cement properties. The dissolution of silica in the water on the action of hydroxyl ions from lime forms chemically active layers which act as

nucleation sites for the hydration reaction to take place. So as more silica gets dissolved, its pozzolanic action is seen where CH is consumed rapidly forming C-S-H phases.

In high strength concrete where the cement content is higher than normal concrete, the addition of SF showed a significant rise in compressive strength. 10% by weight replacement of cement by SF had shown a higher strength improvement than 15% replacement as observed by M.Nili Et al. (2015)[84]. In this work, the researchers studied the properties of silica fume along with nanosilica. They mention about the inter-transitional zone (ITZ) and how that varies by addition of silica fume in comparison to nanosilica. This work concludes that these ITZs which are a result of silicafume and nanosilica additions are what alter the strength properties of the final cement specimens. They had recorded a maximum compressive strength of 44MPa in a nanosilica included sample and concluded that the early age compressive strength was improved more by nanosilica addition than by raw silica fume addition.

2.5.2. Limitations of silica fume:

Since silica fume mainly consists of oxides, the reaction takes time for the silicate mineral to be

released into the hydration matrix. As a result, the onset of pozzolanic reaction is sightly delayed which does not help the initial strength of the material. Also, because of this delayed reactivity, most of the silica fume gets deposited in the pore spaces and acts as a filler instead of effectively taking part in the pozzolanic reaction. Due to this reason, it cannot be considered the most efficient pozzolanic material, but overall improvement of cement properties places it as a very competent cement additive.

2.6. Zeolites:

These are naturally occurring aluminosilicates of alkaline earth metals like potassium, calcium and sodium. They are available in earth's crust in abundance. The variety in the chemical composition

is huge. It can be explored to choose an ideal composition for mixing in cement. Natural zeolites were first discovered in natural basalt formations. At the end of the 19th century, they were also found in sedimentary rocks. This abundance of zeolites in nature makes it a very easily available mineral additive for cement and in more recent years of research, this showed property enhancement in par with the other SCMs used over the years like pozzolans and fly ash.

2.6.1. Advantages of Zeolites:

These materials have been extensively studied, and most recently various compositions have been added to cements to check the effect on the physical properties. Similar to the addition of pozzolanic materials, zeolite addition improves the properties of cement such as workability, fluidity, water content, homogeneity, compactness, as well as the compressive strength. Their property enhancement is in most cases comparable to that of pozzolans. Given the abundance of zeolites, they are considered a better alternative to the pozzolans historically used. Given the ability to engineer the shapes, sizes and compositions of zeolites, they provide a competitive edge over conventional supplementary cementitious materials.

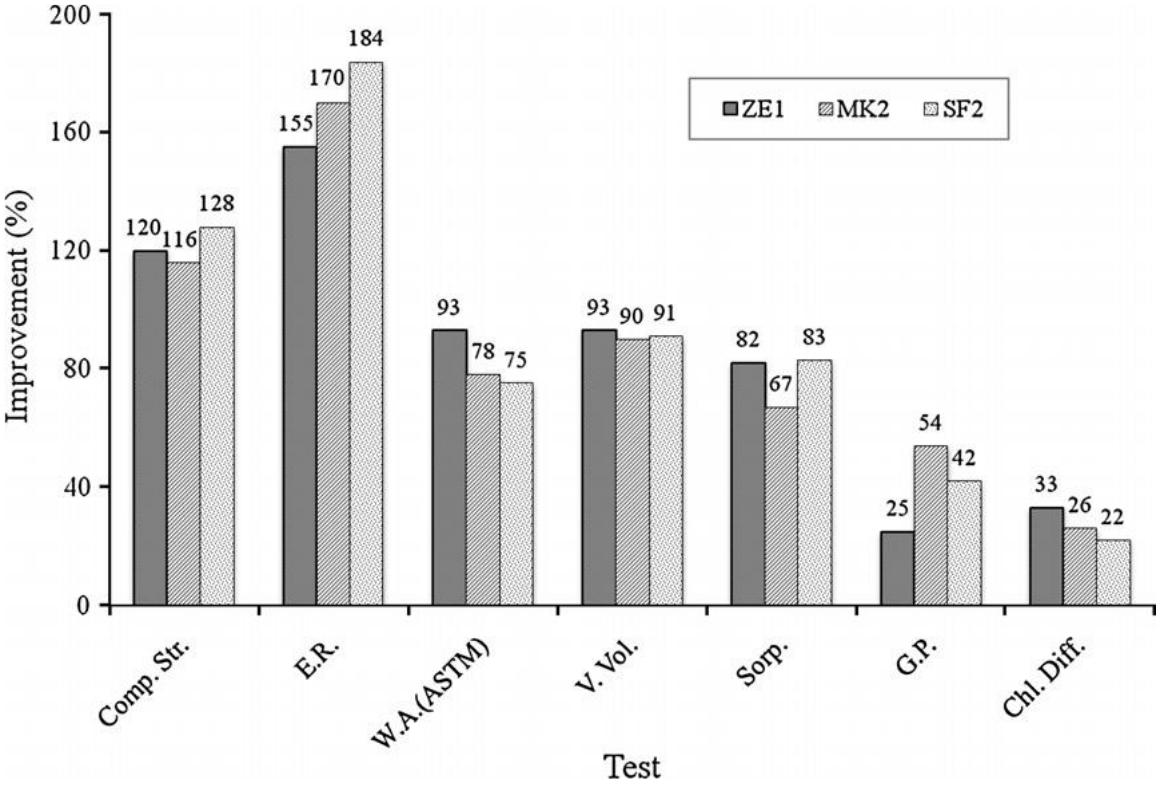

Abbreviatoins:

1) Comp.Str.- Compressive strength;
2) E.R. – Electrical Resistivity;
3) W.A. – water absorption;
4) V.Vol – Void Volume;
5) Sorp. – Sorption;
6) G.P. – Gas permeability;
7) Chl.Diff. – Chloride diffusion.
8) ZE1 – Zeolite 1;
9) MK2 – Metakaolin 2;
10) SF2 – Silica Fume 2.

Fig.2.2: The influence of same replacement level of zeolite in comparison to metakaolin and silica fume on concrete properties [85] The zeolite added cement samples had shown better properties in most of the cases and hence zeolite additions were concluded to show properties in par with the regular cement SCMs if not better than them in some cases.

The physical properties of cement have also been shown to be significantly improved by the addition of zeolites to the cement mixtures. Clinoptilolites were one of the well-known zeolites previously used with cement. A zeolite, ferrierite, has also found application in low density cement formulations used for geothermal wells which is later discussed for its interesting self-healing

properties. Tests have been conducted on usage of zeolites like Mordenite and clinoptilolite. The porous nature of these materials provides large surface areas for the hydration reaction to take place.

The addition of zeolites to cement is shown to have a pronounced effect in resistance to freeze thawing, sulfate attack, chloride permeability, etc. The change in properties of concrete like the addition of pores with occluded air makes the cement resistant to freeze thawing. The change in composition of hydrated cement product with zeolites is also responsible for the cement acquiring various types of chemical stability including resistance to pH, cationic and anionic attacks. Zeolite addition is also shown to have better effect on the strength of cement [86] than the addition of regularly used pozzolanic material additives like silica fume or fly ash [87].

The addition of zeolites was shown to impact the workability, compressive strength, weight, as well as permeability and adsorption properties of resultant cement [31, 88, 89]. The addition of natural zeolites replacing approximately 20% of OPC showed its effect on permeability and other physical properties of self-consolidating concrete (SCC), which is currently widely preferred compared to concrete made by using plain OPC [90]. Hence, it can be said that a huge amount of research has gone into zeolites and their application as mixtures in cement. While part of the research pertains to cement and concrete in general, it's usage in geothermal applications and deep wellbore cements had been a crucial motivation for the testing of this material that would be shown in the process of this work.

Another very interesting observation from prior research was that zeolite addition had shown self-healing properties in low density geothermal cements at high temperatures. This was reported in the work of T.Pyatina et al., [46] where it was observed that zeolite acts as a sacrificial material and as a source of aluminum and silica which help in forming the recovery phases, in other words, self-healing properties. The study was extensive and had a complete breakdown of the phases which formed on self-healing. The main phases observed were a collection of minerals like

magnesium silicates, Aluminum silicates, magnesium aluminum silicates, Calcium aluminum silicates, and calcium aluminum iron silicates. The result was shown in terms of the post-healing strength that the cement samples could achieve. The strength was shown to be regained even after multiple cycles of fracturing and self-healing at geothermal temperature conditions (at around ~270ºC). This formed the basic inspiration for our work, and it would be a promising direction to work in the future to try and replicate similar self-healing at regular GoM (Gulf of Mexico) temperature and chemical conditions like at 90ºC similar to the conditions used for curing our samples in the first place. If this self-healing can be achieved at GoM conditions, zeolite addition would be the ideal solution to achieve zonal isolation in plugging and abandonment applications.

Fig 2.3. Photographs and 3D images of 0·25 mm cracks in clinker/Fer silica-modified or non-

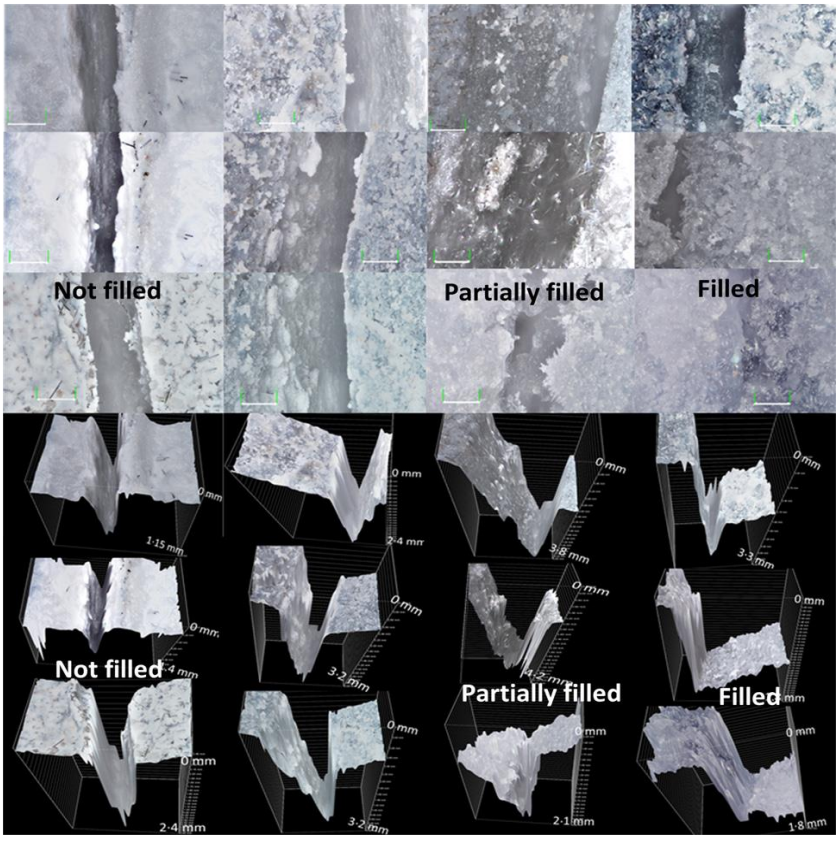

modified samples before and after exposure to water or alkali carbonate environments at 270°C for 1d (control), 5d or 10d showing filled cracks (Reproduced from Pyatina T. Et al.,

2017) [46]. Further studies required to understand the grain boundary interactions of zeolites with cement.

One of the interesting results is the SEM morphological study coupled with profilometry showing the healed cracks and it is shown above in figure 2.3. This shows the healing that was observed at 1-day, 5-day and 10-day periods under alkali environments which are predominant in geothermal conditions.

2.6.2. Limitations of Zeolites:

The presence of various alkali earth metal ions introduces new phases into the cement chemistry. The zeolites are naturally occurring as rocks and hence need to be pulverized or milled into powders to be added into cement, which increases the cost of production. The abundance on the other hand makes up for the cost of extraction of the raw mineral from quarries and takes very little processing. Even in the ground form, the zeolites retain their porous and crystalline nature as they are chemically very stable and the porosity is seen in nano level rather than the micro-level which could be destroyed in the process of milling. The chemical stability of this mineral means that there is very little chemical interaction in the hydration. On the other hand, the porous nature and the presence of alkali-metals in the crystal structure, their ionic nature produces affinity towards the cement phases which are forming and hence act as substrates for hydration reaction to take place improving the efficiency of hydration.

2.7. Gaps in knowledge:

Most of the research performed so far has mainly concentrated on the enhancement of physical and chemical properties of cement and had made hypothesis based on the properties of the additives and possible reaction with cement. Additives like pozzolans and Fly ash had been in use for several

decades and extensive research had been performed on them. The pozzolanic reaction was one of the oldest reactions studied with respect to cement hydration and hence had a clear overview. However, the use of zeolites had been a relatively new area with a limited number of studies on the microstructural properties and hydration of cement. The overall advantage of adding zeolites had been explained in most of the literature, but there is a conflict between whether the zeolites have been an active part in cement hydration like the pozzolans or if they were acting just like substrates. There is a visible knowledge gap in this area and needs further research to get an understanding.

The literature survey provides an insight into the various supplementary cementitious materials that are used, their advantages and disadvantages and finally suggests why we chose zeolites as our ideal additive for our application of cement in plugging and abandonment. Since zeolites have recently gathered interest as SCMs and their working mechanism is not completely explained, this study would be concentrating on understanding the mechanism to recommend the material. In short, the summary of the literature is provided below in table 2.1. showing the advantages and limitations of various mineral admixtures/Supplementary cementitious material (SCM) namely Pozzolans, Blast furnace slag, Fly ash, Silica Fume, and zeolites.

Table 2.1:

Materials	Advantages	Limitations
Pozzolans	• Natural minerals • Abundant resources • Improve strength properties [4] • Reduce porosity and permeability [5]	• Prescence of unreactive glass phases • Require activation in some cases for better performance • Lower early stage strength.

Blast Furnace Slag	• Industrial waste – abundance • Showed better performance than Pozzolans (Deboucha W. et al., [6])	• Predominantly oxides – low reactivity • Poor quality control
Fly ash	• By-product of Coal electric generators. • Reduces porosity and permeability [7] • Improves strength [8]	• No positive effect on hydration – Noted retardation in some cases • Typically act as fillers, so higher percentages are bad for strength.
Silica Fume	• Industrial waste – high availability. • Strength improvement. [9]	• Predominantly oxides – low reactivity • No early age property enhancement • Delayed pozzolanic reaction
Zeolites	• Abundance in nature [10] • Showed properties comparable to other popular SCMs [11-14] • Showed self-healing and enhanced strength properties [15]	• Low pozzolanic reaction • Acts mostly as substrate for hydration • Porous nature of zeolites increases water demand for optimum hydration of cement slurry as it absorbs water.

Table 2.1. (contd.) Summary of literature highlighting the advantages and disadvantages of various SCMs.

CHAPTER III

METHODOLOGY

3.0. Introduction:

This research aims to explore the properties of zeolite to understand its characteristics to explain the mechanism of the zeolite when added to cement. The cement properties are studied and observed with respect to a neat control sample of Class-H cement which is the base case used in our research. The main characterization techniques we use for this purpose are:

A. Morphology, chemical and elemental analysis:

1. TEM (Transmission electron microscopy)
2. SEM (Scanning electron microscopy)
3. EDS (Energy dispersive x-ray spectroscopy)
4. XRD (X-ray diffraction)
5. XRF (X-ray fluorescence)
6. Raman spectroscopy
7. CT (Computed tomography).

B. Petrophysical properties:

1. Porosimeter
2. Permeameter

C. Mechanical properties:

1. UCS (Unconfined compressive strength)
2. Triaxial test
3. Micro and Nano-indentation

The first part of this research involves the characterization of the zeolite. To perform this, we first need the sample preparation of zeolites for various tests. The samples are prepared in two ways. One is the powdered samples for tests like XRD, SEM, TEM, and chemical sensitivity analysis by exposing the powdered samples to various sub-surface chemical conditions and conditions mimicking cement hydration. The second type is by dicing the samples with a minimum of two parallel surfaces and polishing one surface up to a uniformity of ~0.6-1µm. For cement, similar sample prep was used. Powdered samples of neat cement and hydrated cement were taken for XRD while polished cement cores were used for various tests including SEM, EDS, Raman and indentation. Polishing in both cases is performed using an Allied Multiprep™ polisher to a uniformity of ~0.6-1 µm. Crushing the bulk samples to obtain the powders was some using SPEX ball mills. Cylindrical cores of the cement designs are made by putting the respective cement slurries in molds. The zeolite (ferrierite in this study) was added at 5, 15, and 30% by weight of cement (bwoc) as a micronized powder. 0.25%bwoc D-air 5000(Halliburton), 0.30% bwoc dispersant CFR-3 (Halliburton), and bentonite (Performance minerals LLC) at 2.0% bwoc were added to make cement slurry of density 16.4ppg (1.94g/cm3) and water to cement ratio of 0.38

3.1. Sample preparation:

The cement cores are prepared according to the standards from API 10B for wellbore cements. First, the cement slurries are prepared by the following steps:

1. Hand-mixing the Class-H cement powder, respective additives (KCFR-3, Bentonite, D-air-5000) and, micronized zeolite powder.
2. The mixture is then gradually transferred into an industrial blender with calculated amounts of water being mixed at slow speeds (~5000-6000 rpm) within 15 seconds.
3. Once the entire contents are in the blender, the lid is closed, and the blender is turned to high-speed (~12,000 rpm). Care is taken that no lumps are formed in the slurries.

Once the slurries are prepared, they are taken into the respective molds for hydration. KCFR-3 and D-air 5000 were obtained from Halliburton. Bentonite was obtained from performance minerals LLC. The molds used are of 1-inch diameter and 2-inch length for all the permeability, porosity, flowthrough and UCS tests. 1.18inch diameter by 2inch length for Triaxial tests. The rest of the slurry is taken in 2inch diameter molds and other miscellaneous molds for other tests like indentation, Raman, SEM, EDS, etc.

The samples are planned to be prepared according to the following experimental plan. The initial plan was to test two different zeolites in varying percentages by weight of cement namely 5%, 15%, and 30% woc. Following is a table for the division of prepared cement samples for various tests.

Test		Neat Class-H	Ferrierite			Test
		0%	5%	15%	30%	
		16PPG	16PPG	16PPG	16PPG	
UCS	Dry	6	6	6	6	XRD
	Wet	6	6	6	6	
Porosity		3	3	3	3	Indentation
Permeability		3	3	3	3	
Microscopy		2	2	2	2	Microscopy
Total		20	20	20	20	80

Table-3.1. Experimental plan for the cement cores and number of cores required for the tests.

3.2. Sample testing (Experimental techniques):

Initial tests for one zeolite ferrierite were performed by taking a powdered sample of ferrierite with a particle size of up to 425 µm. These samples were immersed in various chemical solutions as shown in the table below.

Condition	solution	Quantity
Alkaline fluid	~ pH 13	0.5gms of $Ca(OH)_2$ in 500mL DI water
Acidic fluid	pH 0.1	1N HCl (as received)
Salt rich fluid	pH 7	17.5gms of NaCl in 500mL DI water
Water	pH 7	DI water 500mL
Organic fluid	NA	Synthetic Mineral oil 50mL

Table-3.2. The chemical solutions used for testing the stability and chemical properties of the zeolites.

Once the powdered zeolites were taken into the above solutions, they were sealed and placed in an environmental chamber at 90oC and 95% Relative humidity for a week simulating a subsurface condition. Once the samples are taken out, various tests are performed including SEM, EDS, XRD, etc.

3.2.1 Chemical and Morphological characterization:

3.2.1.*a.* X-Ray Diffraction (XRD): X-ray diffraction analysis (XRD) is a technique used for studying the cement phases [14, 91]. XRD for the powdered samples was performed using a *Bruker D8 advanced X-ray diffractometer*. This technique was used to do a phase distribution analysis of our samples and in the case of zeolites, to assess and confirm the identity of the zeolite and also observe the phase properties after exposure to various chemical conditions. The powdered samples were made into pellets and taken into the respective sample holders for XRD. The processing of XRD data was done using Profex software (Version 4.1.0) which performs peak matching and

refinement of the XRD peaks. This is done by the mineral and crystal data matching from the software's BGMN database. JCPDS data was also utilized to get the exact peak values of zeolites for initial studies. This is a very important characterization technique to observe the phases based on their crystal structures. The intensive research done by many researchers in the past helps in getting the growing database which is internationally accepted as a tool to identify any phase that is observed during XRD analysis.

3.2.1.*b*. Scanning electron microscopy (SEM): SEM is one of the very important tools to study the microstructure of cement [14, 16, 24]. SEM and EDS were conducted by using the *FEI quanta 600 scanning electron microscope equipped with a Bruker EDAX system for EDS*. In the later stages of our studies, *Thermofisher Scios 2 dual beam SEM* with FIB capabilities was also used. SEM is used to take high magnification images of plain polished zeolites, chemically treated zeolite powders, polished cement cores to observe the morphology. This technique produces very high-resolution micrographs that are obtained at micro and nano scales from the detected secondary and backscattered electrons that are a result of exposure to an electron beam. This is a very crucial characterization technique to identify phases comparing the results to the observations from the literature. This gives the work a very important insight into the morphological characteristics of the various phases present in the cement matrix including hydrated phases, unhydrated phases, and also the new phases introduced into the cement-like zeolite in the case of this research. This can be used to study the grain boundaries within the matrix to hypothesize on the possible mechanism in which the phases interact. This can be supported by the next characterization technique which will be used in conjunction with the SEM.

3.2.1.*c*. Energy dispersive X-ray spectrometry (EDS): EDS was done on the same samples by using the aforementioned set-up to obtain an elemental analysis by mapping the distribution of various elements in the sample giving an estimate of the distribution of phases. In this technique, the materials are characterized based on the x-rays emitted from the material on exposure to the electron beam of the SEM. These emitted x-rays are characteristic to various elements as they

correspond to the excitation and emission of electrons from the various shells of an atom. Based on this characterization technique, we can get an understanding of the elements that are present in a given area and this would help us predict the phases that are being observed under the electron microscope. The results can be obtained as atomic percentages of the elements in question giving us an accurate depiction of the phase distribution in the sample being observed. In this research, we use this technique to differentiate between the various phases that are present in our cement samples giving us an insight into the mechanism of cement hydration and how it is affected by the introduction of additive minerals.

3.2.1.*d.* Transmission electron microscopy (TEM): This was done using *JOEL JEM-2100 STEM a transmission electron microscope.* This was used to observe the crystal structure and morphology of the pure ferrierite powders obtained by crushing the ferrierite sample rocks. These crushed powder samples were transferred on to a TEM grid after sonicating them in isopropanol to get an even distribution of particles on the grid. This is a technique that is similar to SEM but can achieve a much higher resolution as it produces micrographs that are a result of electrons transmitted through nanoscale materials. This can be used to observe materials at the order of a few nanometers making it a preferred technique to observe nanoscale materials over SEM.

3.2.1.*e.* Raman spectroscopy: Raman spectroscopy of the samples was done using the *WiTec alpha-300 tabletop Raman spectroscope*. This is another technique that had been used for cement characterization since late 90s and is recent [27, 92-97]. Raman uses Laser radiation to excite a material and observes the change in the wavelength of the emitted electromagnetic radiation from the material. This corresponds to the vibrational states of the atoms present in a given phase and characteristic peaks are observed for different materials. For our studies, a 532nm green Laser was used for the chemical characterization. Large area scans are obtained to get a profilometry image and single point scans are done to obtain the Raman peaks of the samples.

3.2.1.*f.* X-ray fluorescence (XRF): XRF was also performed for these samples. This is another useful non-destructive characterization technique to know the distribution of oxides and other

chemical components of a cement sample or one of its additives [98]. An *Orbis Micro X-ray Fluorescence Microscope* was used for this characterization. This technique differs from XRD as it observes the x-rays that are a result of fluorescence providing the chemical characteristics rather than the X-rays reflected off a lattice structure which is characteristic for crystals.

3.2.1.*g*. Computed tomography (CT): This is a widely used technique to study the internal and 3-dimensional morphology of materials. It is a non-destructive technique that uses x-rays to take a series of images from around the sample rotating it 360° and reconstructing those slices to form a 3-dimensional volume. A *Yxlon FF20CT* machine, as well as the CT facilities at NETL were used to obtain these results. This is a very useful technique to look at the internal morphology of material, especially pore spaces and even fracture patterns. In this research, current studies include CT imaging after sample failure post-triaxial test to see which material had the least fracture density. Future studies are planned to look at self-healing of the cement plugs and this is a technique that would be indispensable.

3.2.2 Mechanical characterization:

3.2.2.*a* Micro-indentation: This is a characterization technique used to obtain the material strength properties like hardness and calculated elastic modulus from the load curves that are obtained from the indentation. Indentation was performed using the *Nanovea 1000 Micro-nano indenter*. This instrument could perform both micro and nano-indentation, but our studies were limited to the micro-indentation procedure in the initial research. This technique uses a diamond indenter tip that approaches a material and loads the material at a set force and unloads as soon as it reaches the max force specified for that material. These loading and unloading forces are plotted with respect to the depth reached by the indenter (Force Vs displacement curve) during this process which would be used to calculate the strength properties of the material [99]. Care must be taken that the samples used for indentation must be highly polished so that the properties would not vary based on the morphology but due to the material phases. This technique can be used to estimate the average hardness and elastic modulus of a material either at a microscale or at a nanoscale.

3.2.2.*b* Unconfined compressive strength (UCS): UCS of the cement samples [100, 101] was done using a servo-hydraulic computer-controlled load frame from James Cox and Sons. The steps for this were as follows:

- The samples were cut with 2:1 aspect ratio per ASTM standards and ground parallel to within 1 thousandth/inch. Pre-test dimensions of the cement cores and their mass were measured for piston control settings. Samples were loaded at constant strain rate, 1e^-5/sec. The load was applied in the following manner:

    1) load piston actuated in stress control until 50 psi reached.

    2) The piston was then switched to strain (position) control.

    3) The sample is loaded at a constant rate until failure, and then unloaded.

    The peak stress condition was calculated from load cell force measurement and sample diameter.

3.2.2.*c* Triaxial strength testing: Triaxial tests were also conducted for different samples. A temperature-controlled Hoek-type triaxial compression cell was used for these tests. The triaxial cell consists of three main parts: axial deviatoric loading system, confining pressure system, and a temperature controller. In this test, downhole conditions are simulated by creating confining stress and elevated temperatures. Deviatoric stress controlled by the INSTRON-600DX system (Max load-600KN) was applied in a gradually increasing manner until the specimen fails while the confining pressure and temperature were applied. A high-pressure syringe pump is used to maintain the desired confining stress. In the experiments performed for this work, confining pressures of 13.7MPa were applied, allowing precise measurement of the volume change of the specimen associated with it. A controlled temperature of 90 °C was provided by wrapping the Hoek cell with a heating tape. Using this technique is the most equivalent to simulating the stresses that are

observed in the sub-surface and hence it is considered the most wholistic strength test pertaining to our research in hydraulic barrier materials.

3.2.3 Petrophysical/hydraulic property testing:

3.2.3.*a* Porosity: The porosity of the samples was measured using a Corelab ultrapore-300 porosimeter. This is a Helium gas expansion porosimeter used for grain volume and pore volume measurements. The software interface calculates the porosity of the samples using the GV and PV data obtained. Mercury intrusion porosity (MIP) was also used to validate the porosity of the cores in comparison to the helium gas expansion porosimeter.

3.2.3.*b* Permeability: Permeability tests were conducted using Corelab Nano-perm permeameter. This is a helium based permeameter where the permeability of the cores is measured by passing helium through them at constant pressure and observing the differential pressure over a period of 24 hours for the transducer to show constant permeability reading. The data acquired would be averaged later removing the outliers which gives us the average permeability measurement. In the later stages of our research core flooding tests are planned to be conducted using the Corelab AFS 300 core-flooding system giving us the liquid permeability that would be even helpful to arrive at a conclusive statement.

Apart from these, techniques like CT scanning were used to look at the overall 3d morphology of these cores and studies are underway to observe the cement cores before and after a fracture as a result of triaxial testing. Some initial test results with CT scans post triaxial testing are provided in this document. Future work is planned in these lines, and it would be very useful in the further examination. An addition of flowthrough testing within the CT scanner would be able to provide us insight into self-healing. This could be an interesting and highly useful way forward in future work.

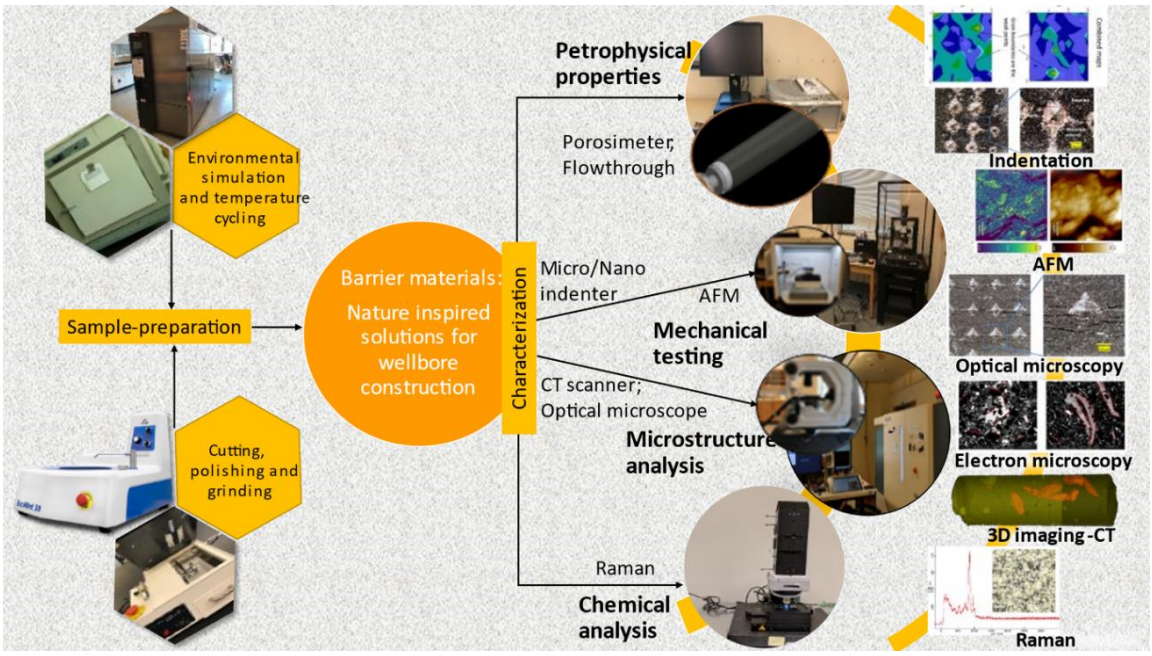

Fig-3.1. Flow chart showing the various characterization techniques used to perform the chemical (XRD, EDS and Raman), microstructural (SEM), mechanical (indenter, UCS and triaxial testing) and petrophysical/hydraulic property characterization (porosity and permeability) of the cement.

The SEM and EDS are used to perform the initial studies on morphologies and chemical composition. During further progress, they would be used to study the morphological and chemical features at the nano or micron levels which could give an understanding of the working mechanism of zeolites. XRD is used to do the phase analysis. Raman is used for characterizing the various phases that are observed in the cement and distinguish each of them. The Raman microscope that is available for our study also has surface profilometry capabilities. CT is used to observe the internal morphology of whole cement cores and the add-on flow-through system helps us understand the petrophysical properties of those samples. Micro indentation was another very useful technique that was used for mechanical testing at micro and nano levels. This was done using a Nanovea pb1000 micro-nano indenter. These studies are very important to study the matrix properties of rock-like materials [102]. Further studies also plan to use techniques like AFM to get a deeper understanding of the materials at hand.

CHAPTER IV

RESULTS

This chapter First Section shows the data acquired from chemical and morphological characterization techniques that are used namely, SEM, EDS, XRD, TEM, Raman and XRF. The initial tests consist of characterization of the additive material chosen for this study namely Ferrierite which is a commercially used zeolite in geothermal cements. Once the additive material is characterized in its pure phase, we get insights into the interaction of this material with various subsurface and cement hydration conditions. We then move on to the characterization of cement samples which have 5%, 15% and 30% ferrierite additions to them. The second section consists of the mechanical characterization that was done on our samples which includes Micro-indentation, UCS and Triaxial test results. The last section consists of the petrophysical characterization of the resultant cement cores. This would be the direction of our future work to try to understand the working mechanism of zeolite and how it works in cement. The results corresponding to these characterization techniques are provided below.

4.1 Chemical and Morphological characterization:

4.1.*a.* Microstructural properties and micro chemical characterization (SEM&EDS):

In figure 4.1 (a-h) below, the SEM and EDS characterization results of our additive material ferrierite are observed under Different chemical conditions namely DI water(Control), low pH (~1),

high pH (~13), Brine solution (35 ppt), and oil as mentioned in the methodology. Figures 4.1 (a-f) show the maps corresponding to the respective ferrierite sample and Figures 4.1g and h are EDS charts showing atomic percentages for each of the samples.

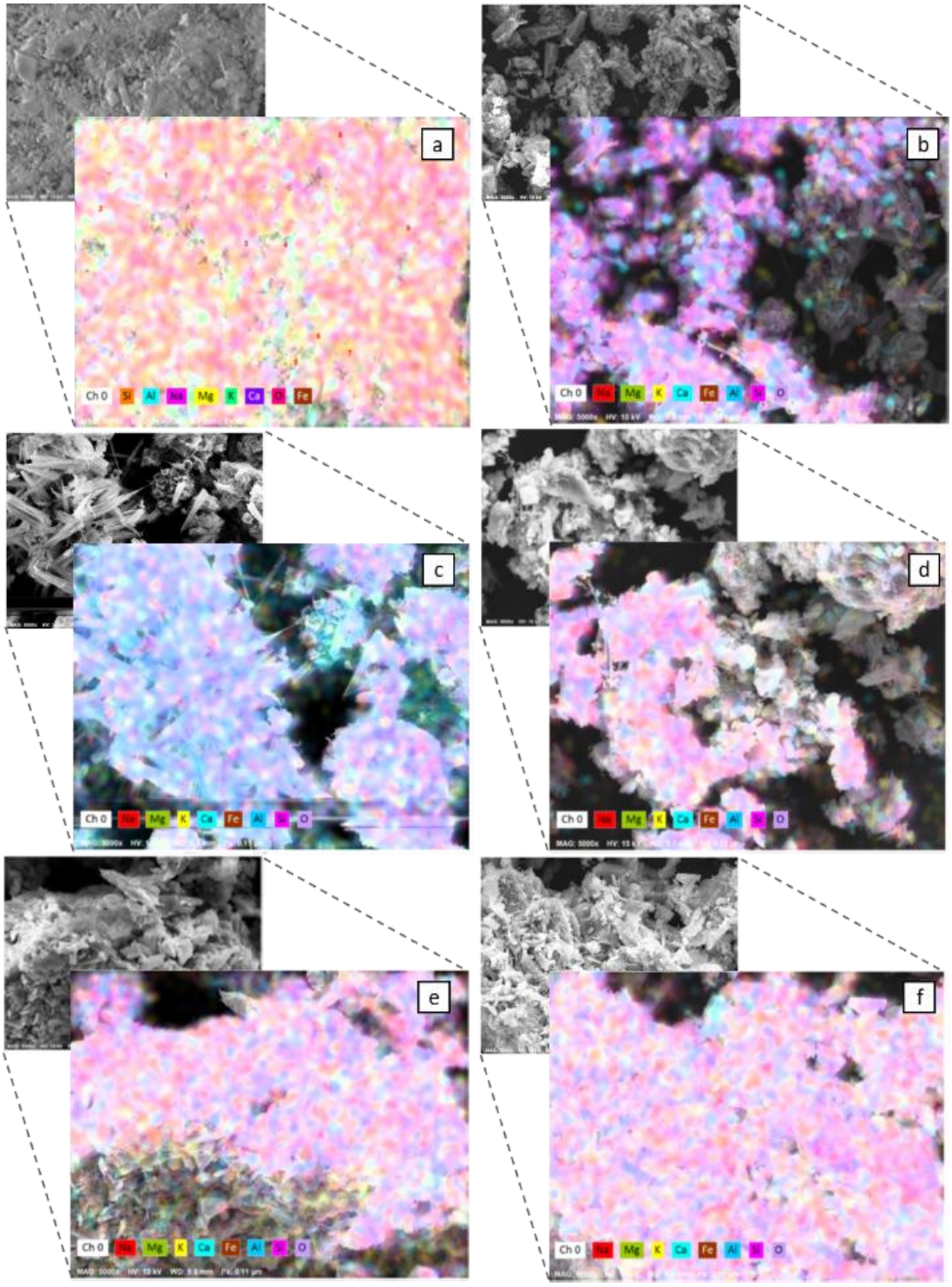

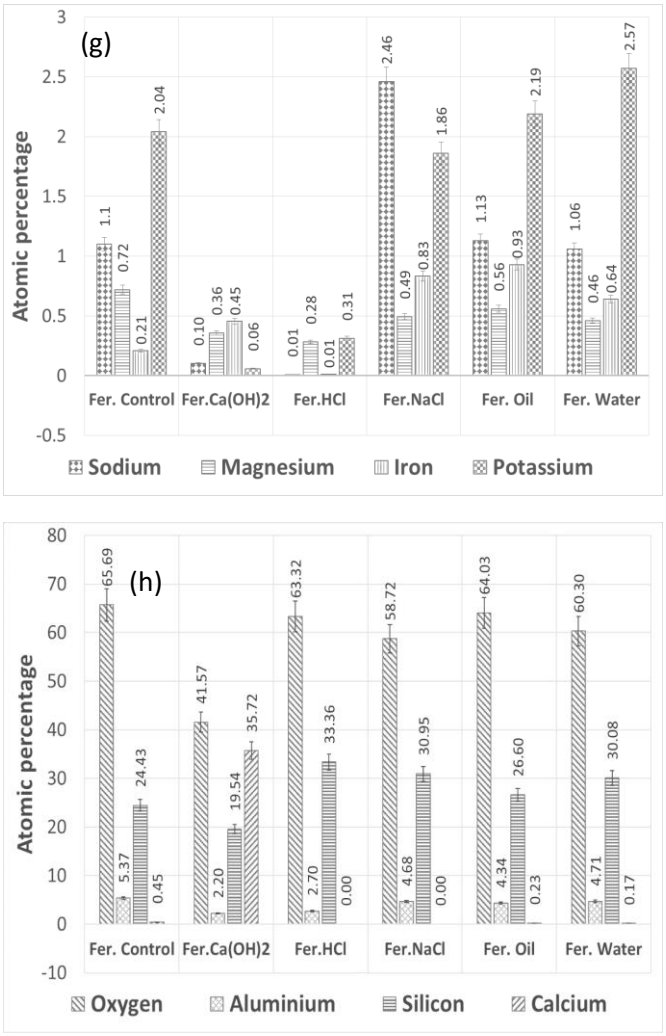

Fig-4.1. EDS maps of chemically treated ferrierite powder at 5000x (a) Plain ferrierite (Control); (b) ferrierite in HCl; (c) ferrierite in $Ca(OH)_2$; (d) ferrierite in NaCl; (e) ferrierite in DI Water, (f) ferrierite in oil. The accumulation of CH crystals on the ferrierite can be observed in the image (c). The corresponding map shows that the content of Calcium (Color coded as blue in the map), is higher in this case. Atomic percentages of various elements are shown in the chemically treated ferrierite powder. The treatment was performed for one week at 90°C. (g) The atomic percentages of the minor elements are seen in this plot. (h) The atomic percentages of the major elements are seen in this plot. The EDS is not quantitative as the surface is not flat, but shows elemental distribution (Vissa et al., 2019)[9]

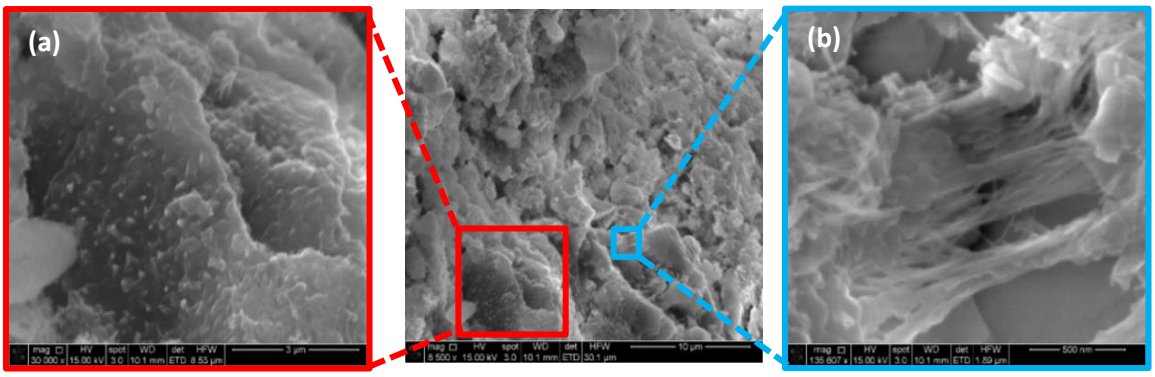

Fig-4.2. Fractured core samples of zeolite cement showing features like (a) 30,000x magnification under SEM showing newly hydrated crystals and (b) 135,607x magnification under SEM morphology indicating possible self-healing properties as secondary hydrated crystals can be seen.

The EDS studies performed above would show us the stability of the elemental composition of our material in sub-surface conditions as well as in cement hydration conditions as we test in high-pH, low-pH conditions. We also test the interaction with brine as the material needs to stay stable in sea water since we are looking at application in offshore wellbores. The control sample is tested with water to see if there was any interaction so that the material would not spontaneously interact with water forming foreign phases which could be deteriorating to cement when it is added to the cement. Last but not the least, ferrierite is tested for interaction with oil to account for accidental hydrocarbon interaction of the cement plugs and also to see if there is any effect due to oil-based drilling mud contaminations which could be detrimental to cement morphology. Figures 4.1 (g and h) show the atomic percentage charts showing the elemental distribution in ferrierite which are mostly in similar quantities on exposure to these chemical conditions showing the phase stability of ferrierite. Figure 4.2 shows high magnification images of a test sample of commercial geothermal zeolite cement which was a commercially available Class-L cement for geothermal well construction which was the base for our study as it showed self-healing abilities. This particular micrograph shows the morphology that suggests self-healing.

Figure 4.4 shows the XRD results of the same ferrierite samples which were characterized with EDS to support the observation that ferrierite has a very stable phase under all these chemical conditions as EDS was not a valid quantitative chemical characterization. Table-6.1 in the appendix provides the corresponding elemental composition of zeolite. Table-6.4 in the appendix compiles the elemental composition of the zeolite samples exposed to the different chemical conditions. Figure 4.3 highlights a ferrierite grain within a cement matrix that retains the phase composition of zeolite further supporting the claim of phase stability forming the basis for our hypothesis that ferrierite remains stable during cement hydration and acts as a substrate for hydration.

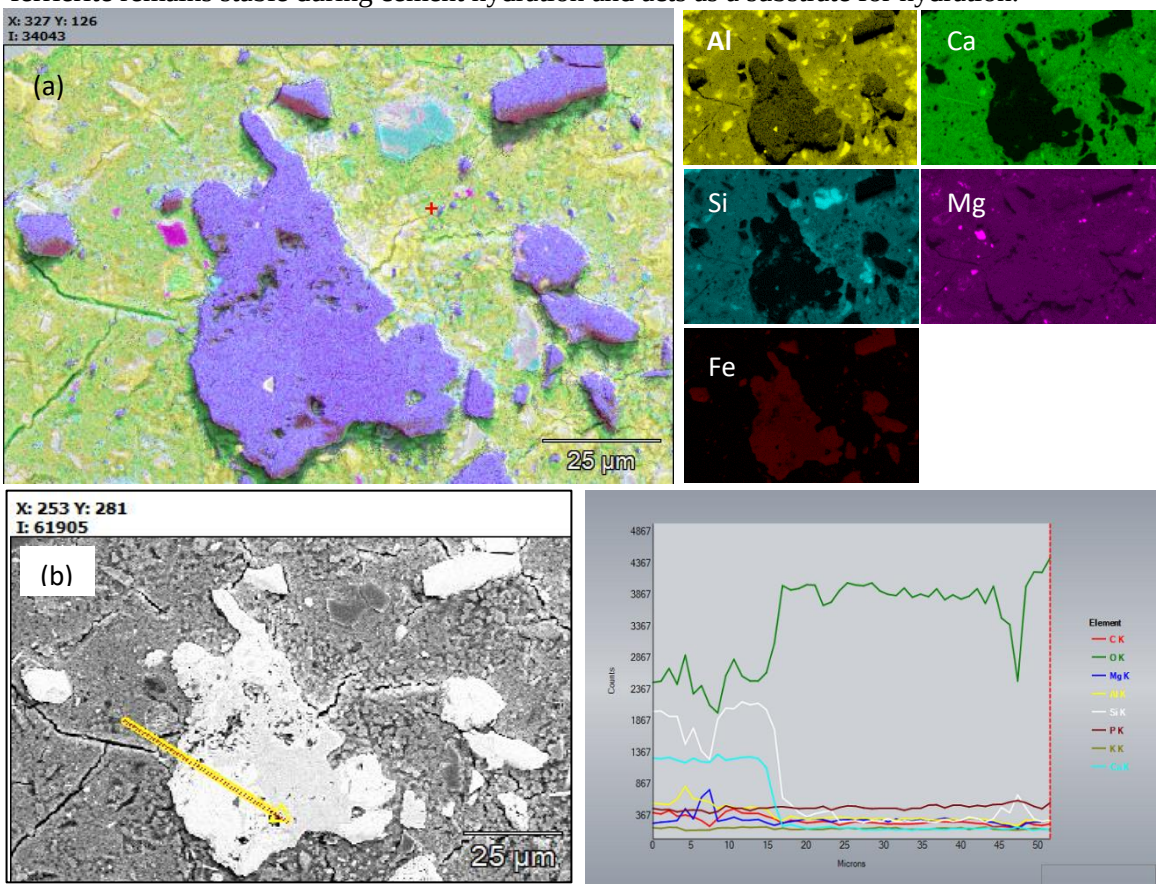

Fig-4.3. Unreacted Ferrierite was observed within the cement matrix of the polished core of commercial zeolite cement formulation. (a) A composite EDS map of feature on the cement surface of a polished zeolite cement core observed at 1500x magnification, highlighting the phase which consists of aluminium, silicon as well as traces of iron and magnesium, with a lack of calcium which is present all throughout the cement matrix, showing that the possible

phase is of Ferrierite which is the zeolite used in this cement. (b) EDS line profile of the feature showing a sharp drop in the counts for Calcium and silicon which are major elemental components of cement matrix showing that this phase is foreign to cement matrix and is most likely a phase formed as a result of zeolite interaction with cement. Also the increase of oxygen content indicates the presence of oxides of aluminium and silicon which are the building blocks of zeolite.

4.1.*b*. Mineral phase characterization (XRD):

The next set of tests include the phase studies which are done using X-ray diffraction (XRD) where mineral phases are identified based on their characteristic peaks at the respective 2Θ values plotted against intensity. Figue 4.4 below shows the phase characteristics of the mineral ferrierite which was observed to be stable post-exposure to chemical conditions seen in the subsurface and during hydration. The peaks corresponding to ferrierite are highlighted in the figure. There is also a calcite peak that was observed in the ferrierite sample exposed to Calcium hydroxide solution indicating the formation of calcite crystals on top of the mineral surface as had been observed in the SEM images. This indicates the affinity of ferrierite to calcium and is supportive of our hypothesis that ferrierite acts as a substrate for hydration to occur. This is based on the fact that Calcium is a very dominant element in the hydration reaction and its byproducts – the cement phases. This is further strengthened by observing the XRD for hydrated and unhydrated cements with and without zeolite where the zeolite (Ferrierite) peaks are still observed in the zeolite added cements before and after hydration. Figure 6.4 in the appendix represents the raw data which is hyperlinked in the corresponding figure caption. This is one of the main findings of this study strengthening the hypothesis and having been consistent with respect to SEM and EDS.

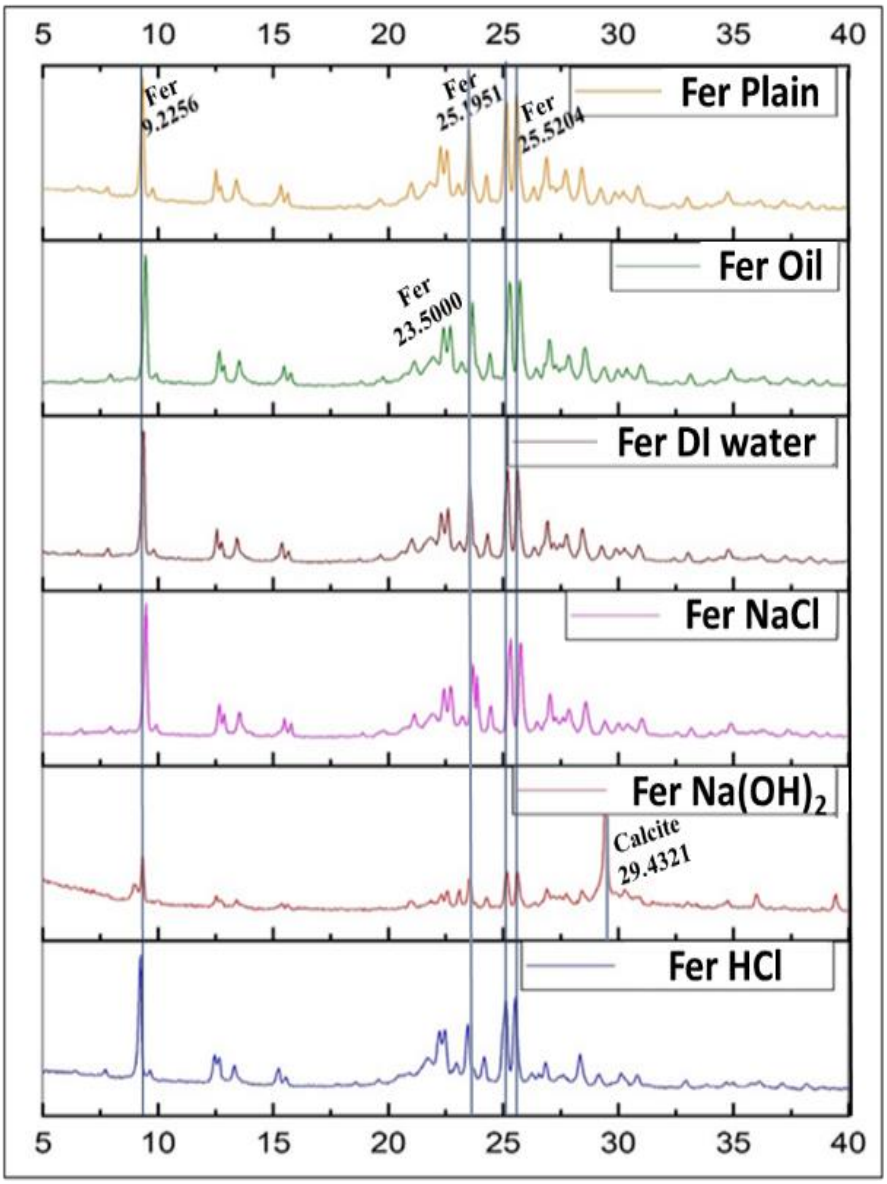

Fig-4.4. XRD analysis of chemically treated ferrierite powder in various sub-surface chemical conditions. The phase compositions remain consistent with an exception of CH peaks from unreacted CH deposited on the ferrierite after suspending it in $Ca(OH)_2$. The XRD peaks characteristic of ferrierite-Mg are seen at 2θ values of 9.2256, 23.5000, 25.1951 and 25.5204. while an extra calcite peak is observed at 29.4321 showing the ferrierite's affinity to calcium hydroxide inferring that it will be attracting cement phases during hydration. (Vissa et al., SPE HSE, 2019 published)

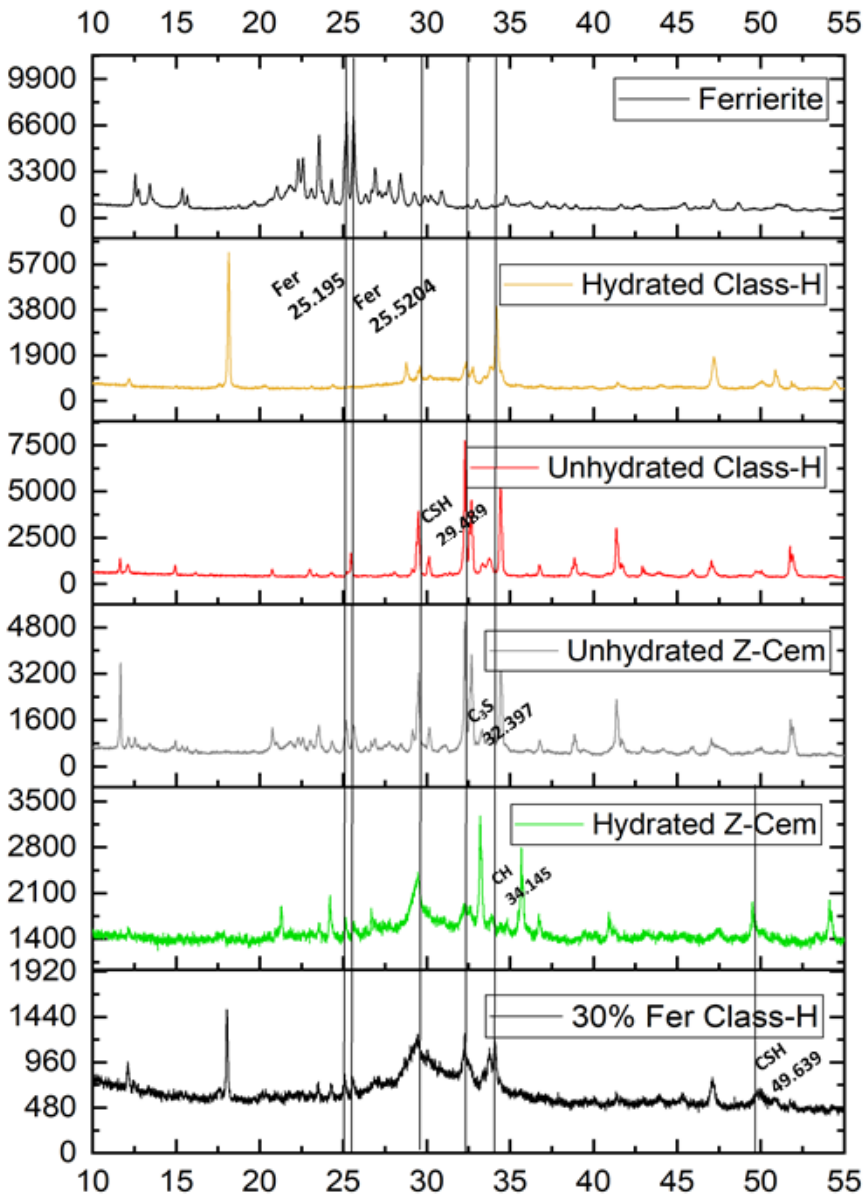

Fig-4.5. XRD results showing Phase comparison between ferrierite, hydrated class-H, unhydrated class-H, unhydrated zeolite cement, hydrated zeolite cement and, 30% ferrierite added class-H cement (powdered Hydrated core) suggesting the initial success of Class-H cement design with ferrierite additions. In this graph, the ferrierite peaks (2Ɵ of 25.195, 25.5204) which are highlighted in the ferrierite XRD plot are also observed in zeolite cement and 30% ferrierite added class-H cement. The other cement phases are highlighted to show the phase similarity in the cement matrix.

As observed above in figure 4.5, the comparison is done between hydrated and unhydrated class-H cements with hydrated and unhydrated zeolite cement formulations (FlexCem™) and 30% Ferrierite added cement formulation, showing how ferrierite remains as a stable phase showing characteristic 2Θ peaks even after 28 days of hydration. The peaks of ferrierite observed in cement match with the pure ferrierite phase that was shown at the top of the figure. This further supports our hypothesis and is in line with the observations from earlier XRD and EDS results.

4.1.c. Nano structural morphology characterization (TEM):

In figure 4.6. below, ferrierite was observed as a single-phase under a TEM showing the characteristic crystal structures as observed from literature corresponding to ferrierite crystal phases. Our ferrierite sample is predominantly Ferrierite-Mg as observed in XRD and it is characterized by spherical aggregates of orthorhombic crystals and both these features can be observed in the TEM micrographs taken at 25000x, and 30000x This concludes the characterization of ferrierite in specific and how it interacts with cement. Once this characterization is conclusive, the next step is testing it with cement. As observed from the XRD and EDS results above, ferrierite has a stable phase that stays stable throughout the hydration. This is further supported by Raman results shown in the next section.

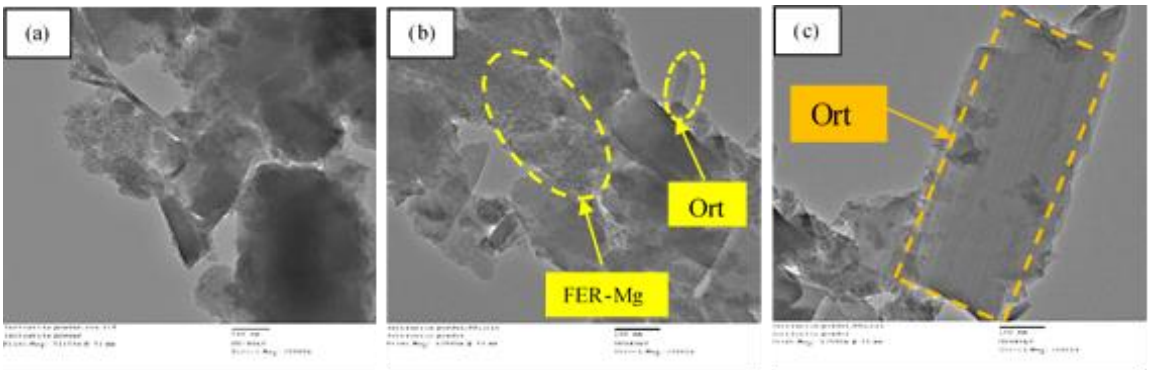

Fig-4.6. TEM obtained for samples of powdered ferrierite at: (a)25000x magnification showing the different morphologies; (b) 30000x magnification highlighting the characteristic

crystal structures; (c) 30000x magnification image focusing on a single orthorhombic structure.

4.1.*d.* Chemical Characterization-I (Raman spectroscopy):

The following figures 4.7.1 - 4.7.4, show the Raman data for 5%, 15% and 30% ferrierite added class-H cement samples are compared to neat class-H sample showing how characteristic ferrierite phases are observed in all the ferrierite added samples which further supports the hypothesis. It also includes a large area Raman scan showing the phase distribution and also giving a profilometric image of the phase morphology.

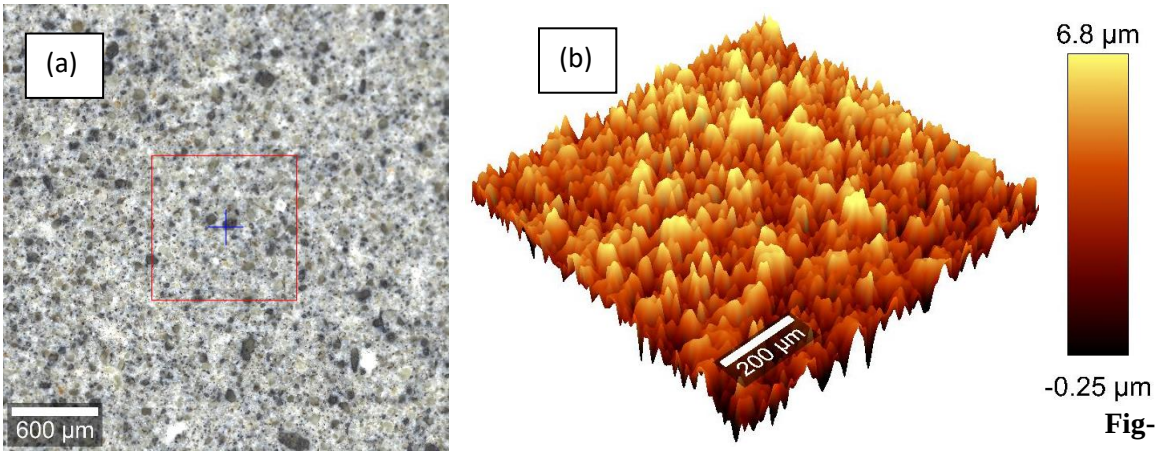

Fig-4.7.1 Raman results for polished cores of Neat Class-H cement (a) Optical micrograph of polished cement core (b) Large area profilometry scan of the cement. (c) Phase peaks at 600-630nm,(CSH) 740nm, (C_3A) 842nm and 972 nm(C_2S) were observed.

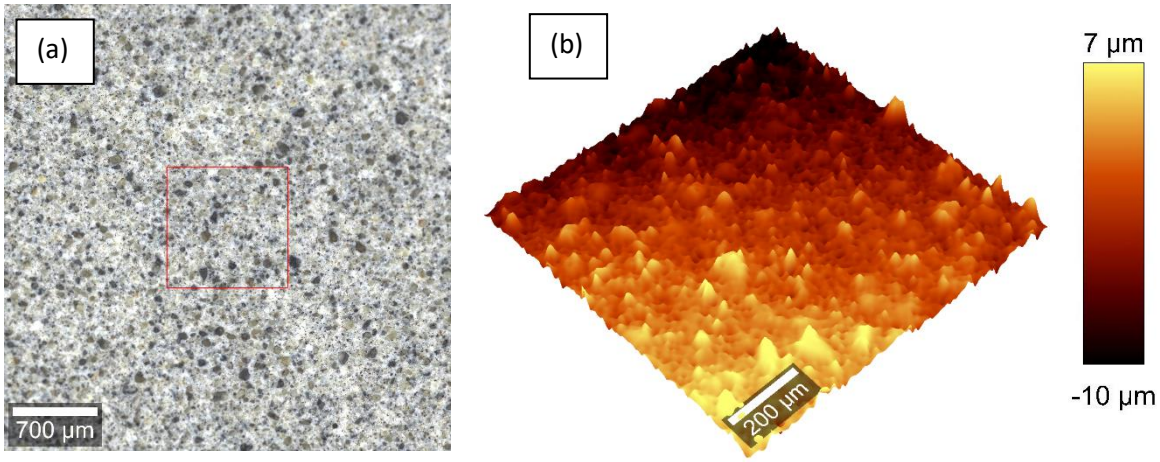

Fig-4.7.2 Raman results for polished cores of 5% ferrierite added Class-H cement (a) Optical micrograph of polished cement core (b) Large area profilometry scan of the cement. (c) phase peak at 416nm, (Ferrierite (Fer)). C-S-H, C_3A and C_2S are the same as mentioned in the plot for neat Class-H.

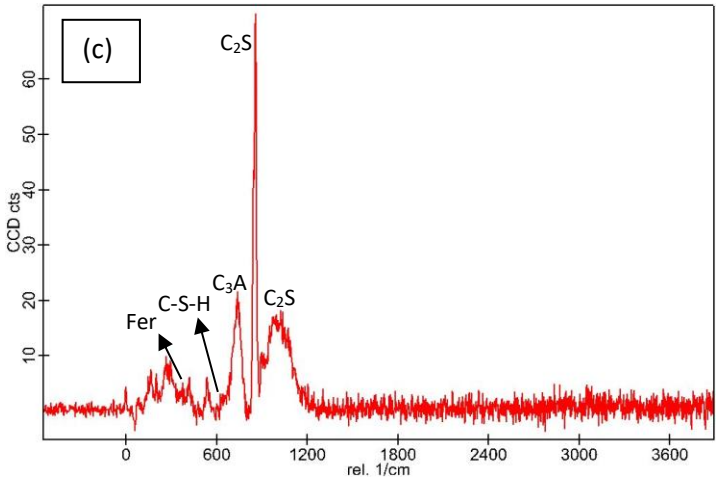

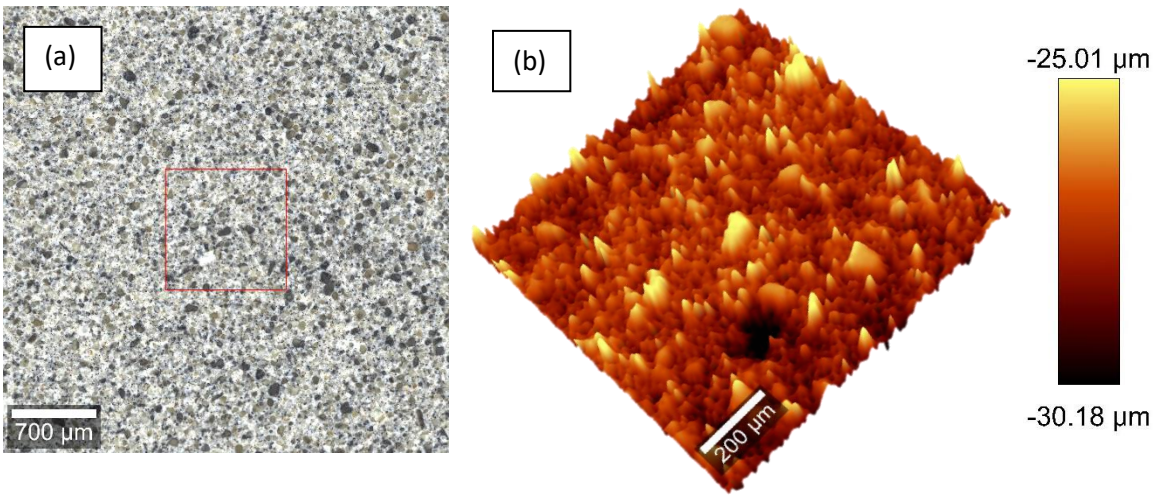

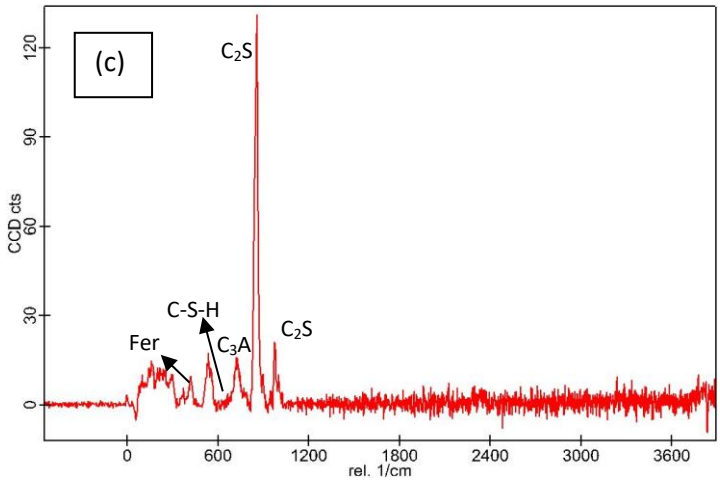

Fig-4.7.3 Raman results for polished cores of 15% ferrierite added Class-H cement (a) Optical micrograph of polished cement core (b) Large area profilometry scan of the cement. (c) Phase peaks identical for ferrierite, CSH, C_3A, C_2S as observed earlier.

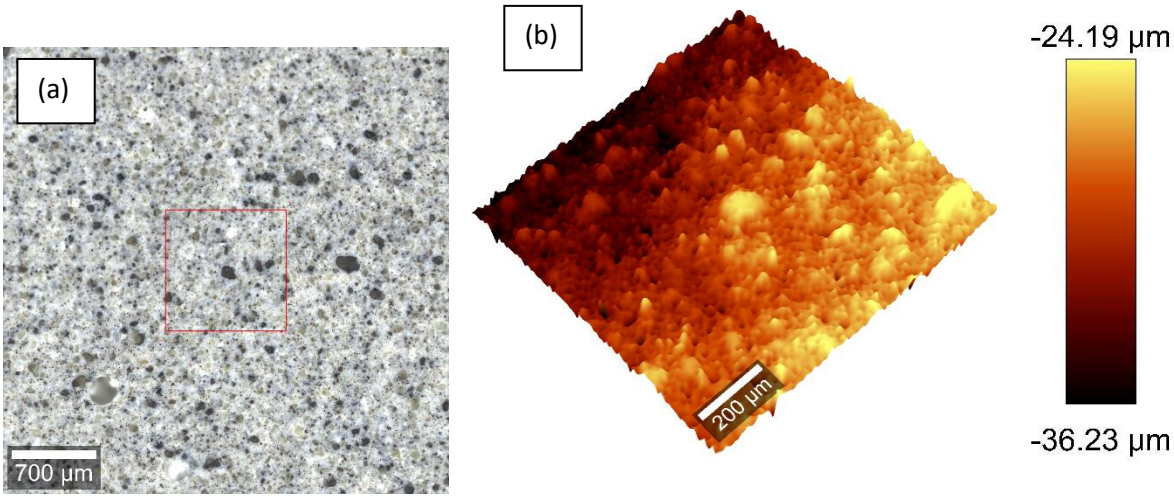

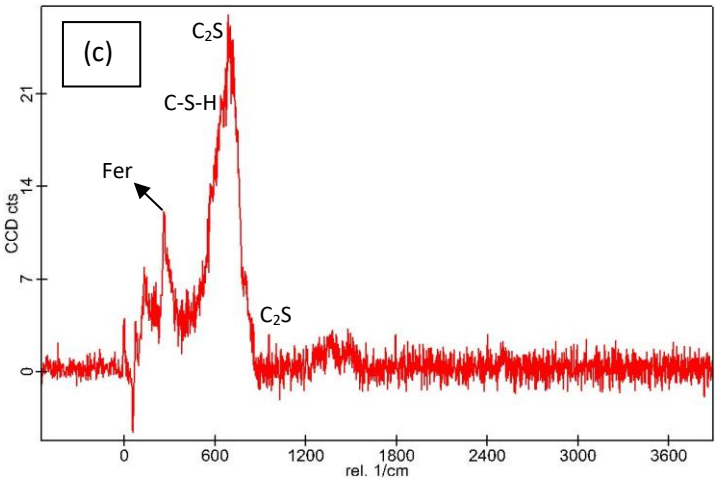

Fig-4.7.4 Raman results for polished cores of 30% ferrierite added Class-H cement (a) Optical micrograph of polished cement core (b) Large area profilometry scan of the cement. (c) Phase peaks for ferrierite, C-S-H and C_2S are observed in this plot. However, C_3A was not resolved well in these scans.

4.1.e. Chemical Characterization-II (X-ray fluorescence (XRF)):

The XRF results are shown in figure 4.8 below showing the distribution of various oxides present in the cement. This is a non-destructive technique as mentioned in the methodology. A table is provided below to show the distribution of the chemical oxides in the material. Corresponding data is provided in appendix tables- 6.6-6.8. This figure shows the comparison between unhydrated class-H cement and unhydrated zeolite cement (commercial geothermal zeolite cement) highlighting the presence of a stable zeolite phase which can be noted from the comparison between the phases of pure ferrierite and that of commercial geothermal zeolite cement.

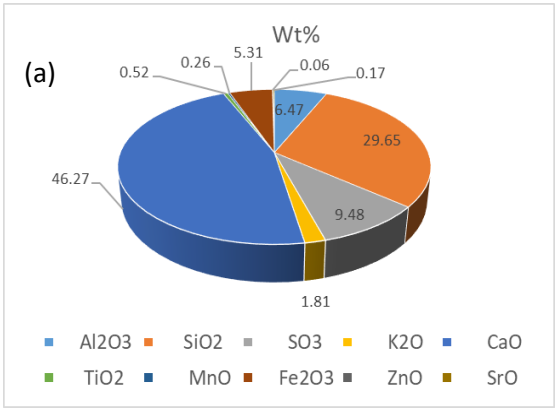

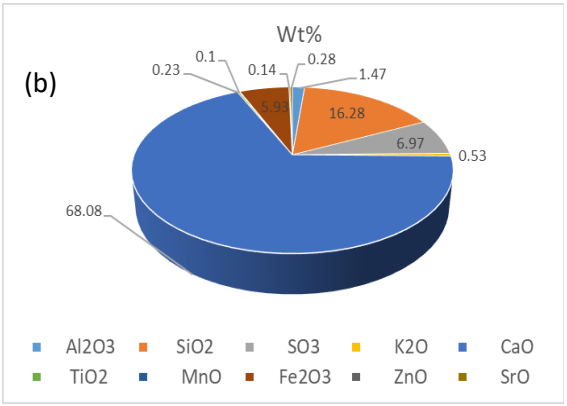

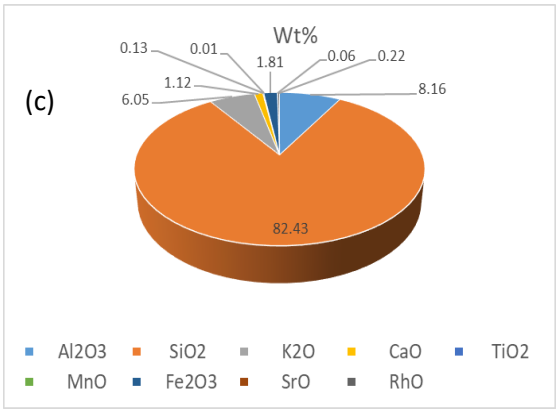

Fig-4.8. XRF results showing the percentage distribution of various oxides present in commercial zeolite cement (a) and plain Class-H cement (b), before hydration. (c) is the XRF data for ferrierite, which is a zeolite. the similarity in phases and or oxide composition indicates that there are no new/intermediary phases that are formed. But the addition of zeolite does reduce the CaO content which would eventually result in the more brittle phases of cement on hydration

Oxide formula	Class-H cement	Commercial geothermal zeolite cement	Ferrierite
Al_2O_3	1.47	6.47	8.16
SiO_2	16.28	29.65	82.43
SO_3	6.97	9.48	_
K_2O	0.53	1.81	6.05
CaO	68.08	46.27	1.12
TiO_2	0.23	0.52	0.13
MnO	0.1	0.26	0.01
Fe_2O_3	5.93	5.31	1.81
ZnO	0.14	0.06	_
SrO	0.28	0.17	0.04

Table 4.1: Oxides present in neat Class-H cement, geothermal zeolite cement (FlexCem™) and ferrierite by weight percent (as represented in the pie charts above)

4.1.*f*. 3-dimensional internal morphology characterization (CT):

The internal fracture morphology of the ferrierite added cement samples was studied using Computed tomography (CT) after triaxial testing which would be shown in the next section. This data on being processed could give us void spaces and other relevant information. Further testing would be required to check the material for self-healing in the future. Figure 4.9 below shows some CT images acquired post triaxial testing. According to the CT 5% shows the best triaxial performance as it has the least fracture density. The supporting data is provided in the triaxial test

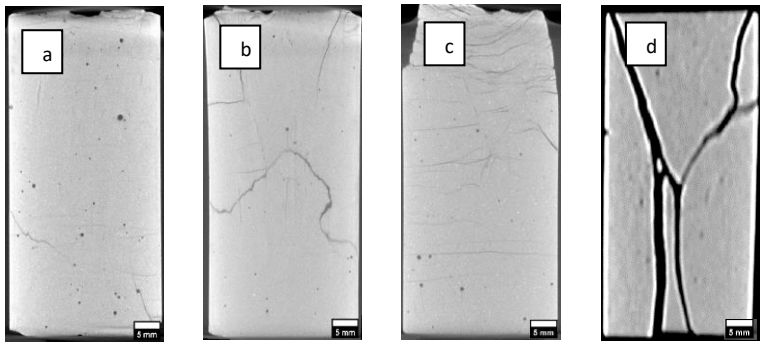

Fig-4.9. CT scans of cement cores after failure under triaxial testing at 6000psi confining pressure and 90°C. a) 5% Ferrierite added cement; b) 15% ferrierite added cement; c) 30% ferrierite added cement; d) Neat Class-H cement showing the failure in comparison to each

other. From the above CT scans, it could be observed that 5% ferrierite added class-H cement cores had the best triaxial strength as they had the least fractures after failure.

4.2 Mechanical characterization:

4.2.*a*. Micro-mechanical characterization (Micro-indentation):

Figure 4.9. below shows a 5x5 indentation grid on a highly polished cement surface for which the obtained hardness and elastic modulus are mapped beside it. This is used to calculate the average hardness and elastic modulus of the sample. The hardness and elastic modulus are calculated from the force Vs displacement curves obtained from each indent by the software interface of the indenter. They were further processed by mapping the hardness and elastic modulus corresponding to each indent and represented as mentioned above. These indent marks were also observed under SEM to obtain the morphology and also the chemical characterization using EDS to show the phase stability of cement phases under stress. This test would be more useful to observe self-healing after the failed cores are kept in the environmental chamber again at high temperature and humidity conditions similar to the ones used for hydration and curing of the cement cores. Self-healing would possibly occur due to secondary hydration and the corresponding phase changes would be visible in the EDS maps acquired for the indenter marks post-curing.

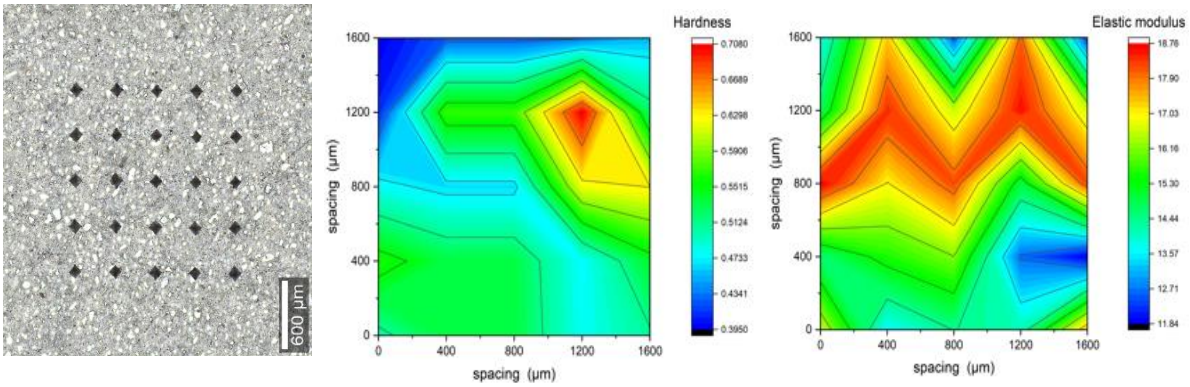

Fig-4.10.1. Indentation results for Neat cement polished cores with 25 indents and maps of hardness (Avg 0.506 GPa) and elastic modulus (Avg 15.72 GPa).

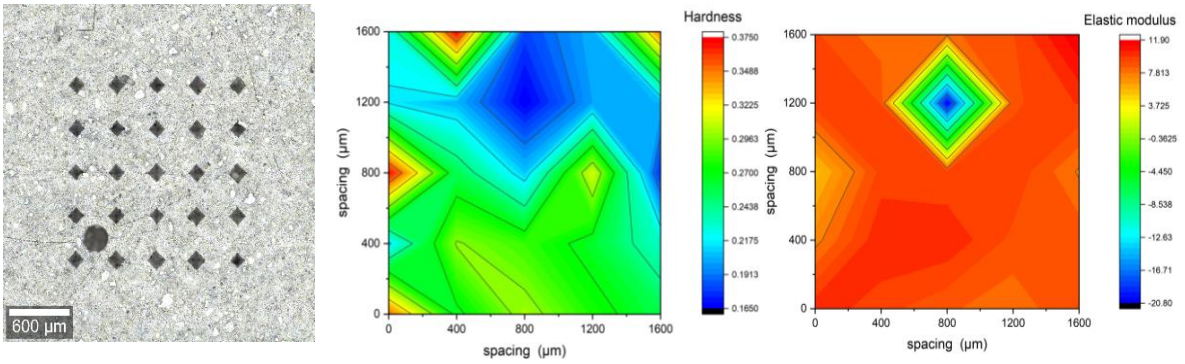

Fig-4.10.2 Indentation results for 5% ferrierite added class-H cement polished cores with 25 indents and maps of hardness (Avg 0.394 GPa) and elastic modulus (Avg 14.03 GPa).

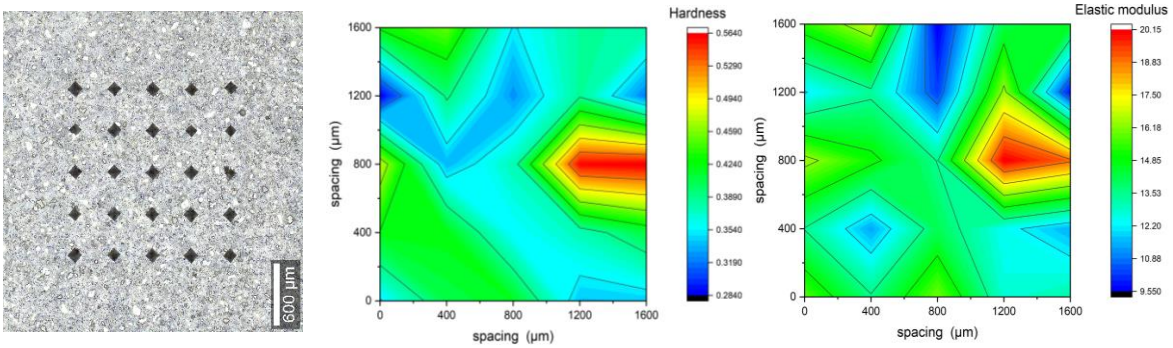

Fig-4.10.3 Indentation results for 15% ferrierite added class-H cement polished cores with 25 indents and maps of hardness (Avg 0.319 GPa) and elastic modulus (Avg 11.01 GPa).

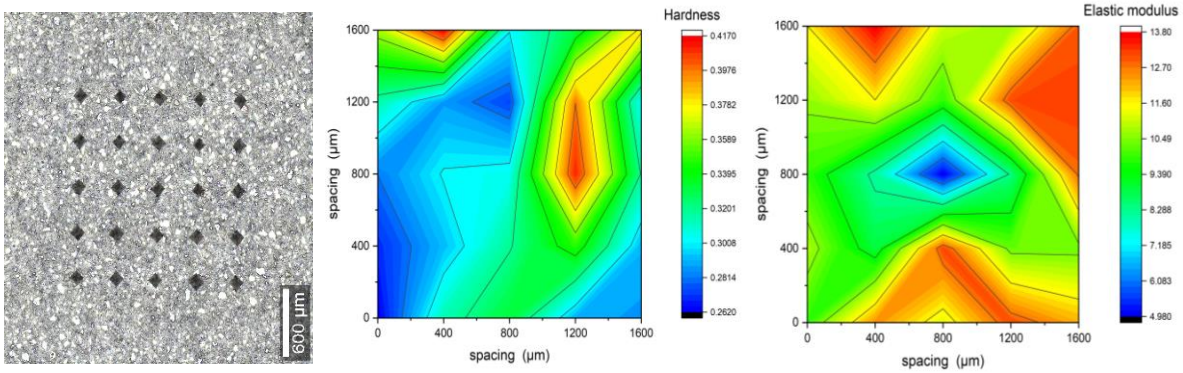

Fig-4.10.4 Indentation results for 30% ferrierite added class-H cement polished cores with 25 indents and maps of hardness (Avg 0.256 GPa) and elastic modulus (Avg 7.88 GPa).

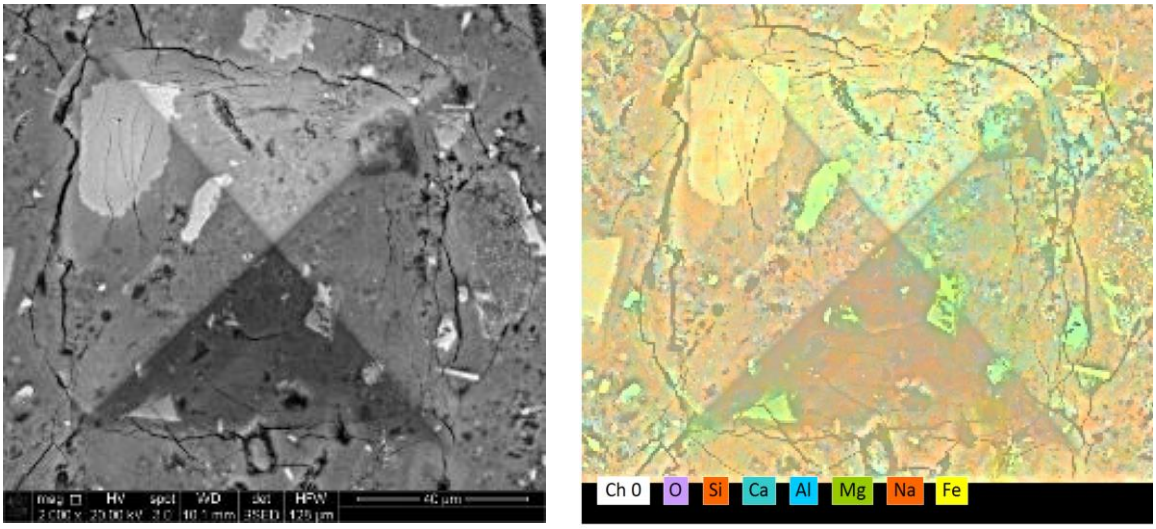

Fig-4.10.5 An EDS map corresponding to an SEM image showing a single indent on neat cement. Indentation was done for the other formulations (for 5%,15%,30% ferrierite added Class-H cement) as well, and SEM and EDS studies are under progress to see if there is any noticeable surface chemical change on failure. (Vissa et al., GRC 2021, accepted manuscript).

Future work is planned to test the indentation marks in a more detailed manner correlating them with the EDS studies to see if there is any chemical change in the matrix. This could help us nail down the mechanism if there is any self-healing observed in the failed samples due to secondary hydration. But the cores that need to be tested would need to be placed in an environmental chamber at high temperature and humidity conditions similar to the ones that were used during curing as mentioned above. The data corresponding to the maps is in appendix tables- 6.10-6.13.

4.2.*b*. Strength Properties Characterization-I (Unconfined compressive strength (UCS)):

This is an internationally acclaimed test to measure the strength of a material and figure 4.11. shows how the addition of 5%, 15%, 30% ferrierite to class-H cement had impacted the mechanical properties of the resultant cement core samples in comparison to neat class-H cement core samples. In this figure, UCS is compared to the hardness and elastic modulus as observed from the indentation testing. While elastic modulus and hardness follow a similar trend with 5% ferrierite

having a little less magnitude compared to neat class-H, UCS results show the highest values for 5% ferrierite added class-H cement cores at 9934.3 psi compared to 7041.52psi for neat class-H cement. With this, 5% ferrierite addition is initially chosen as the better performer within the different ferrierite added formulations. This would be further tested by other mechanical characterization techniques like the triaxial test which is included below in the next section.

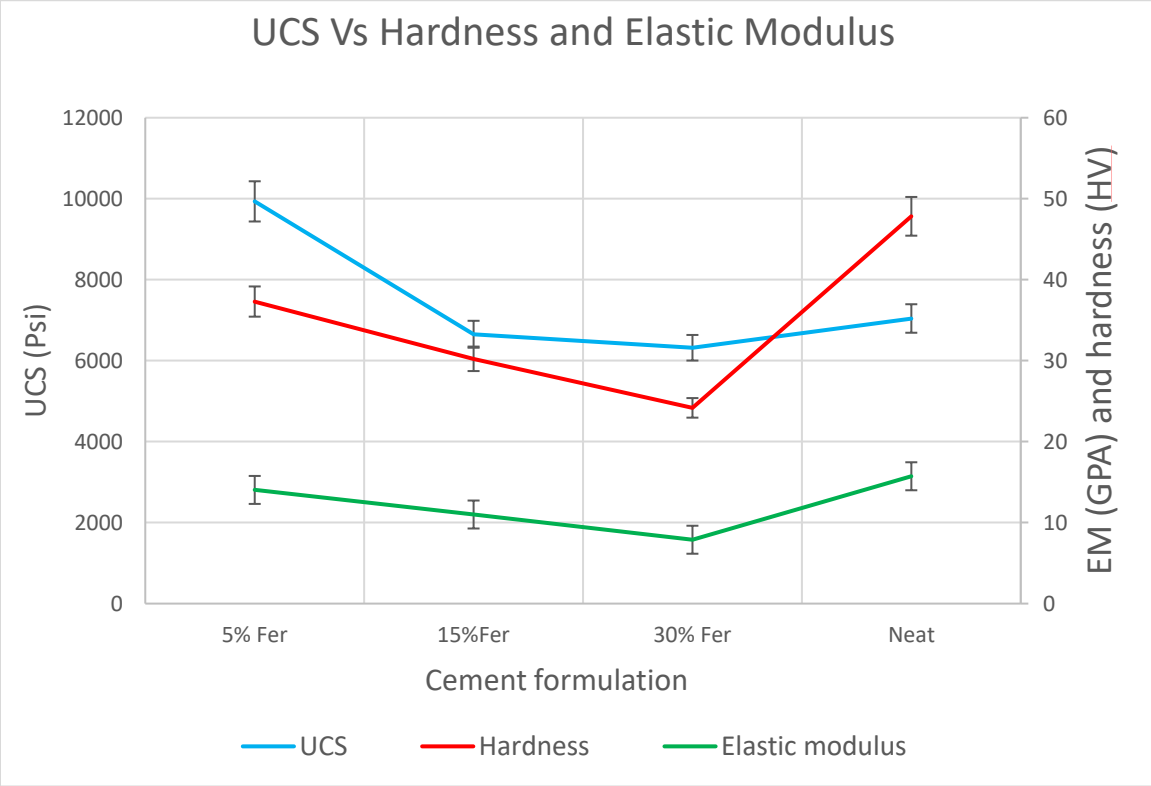

Fig-4.11. UCS Vs Indentation for 5%,15%,30% ferrierite added Class-H and Neat class-H cement showing slightly similar trends. While UCS is the highest for 5% ferrierite added cement at 9934.3 psi compared to neat UCS at 7041.5psi. Elastic modulus and hardness on the other hand are highest for neat class-H with averages of 15.72 GPa (EM) and 47.82 (hardness) followed by 5% ferrierite addition at 14.03 GPa (EM) and 37.3 (hardness). The hardness and elastic modulus decrease gradually with increase in percentage addition of ferrierite which is a similar trend as shown in UCS.

4.2.*c*. Strength Properties Characterization-II (Triaxial strength testing):

This is another very crucial strength test as it tests the properties of material not only under unilateral stress, but by applying triaxial stress on the sample under confinement pressure and elevated temperatures of 90°C which gets closest to simulating the downhole conditions where the material needs to work robustly. Four sample cores with 5%, 15%, 30% ferrierite bwoc additions to Class-H and Neat Class-H Cement slurry designs were tested at the same confining stress (2000psi) and temperature (90°C) conditions. It shows that the 5% FER sample has the highest axial peak stress at 68.8 MPa and the axial peak stress is monotonically decreasing when the FER percentage is increasing. However, the 30% FER sample, which has the lowest axial peak stress among the other two doses, is still showing higher axial stress than the neat cement. Despite that, the young's modulus of neat cement is higher than the 5% FER and 15% FER sample, but lower than the 30% FER sample. Overall, 5% is shown to have the best performance under triaxial testing. For this test, the raw data includes sample height (H) and sample diameter (D), which are the initial measurements taken at ambient stress conditions, lateral pressure (σ_3), axial load (P), axial deformation (ΔL), and the test duration (T). The axial load divided by the specimen's cross-sectional area gives the axial stress. Axial strain (e_A) is estimated by dividing the axial deformation ΔL (obtained from the load frame) with the height of the sample (H):

$$e_A = \Delta L/H$$

Thus, the strain-stress curve of each specimen can be obtained, which is shown in figure 4.12. The initial linear portion of this curve is used to obtain Young's modulus of that specimen.

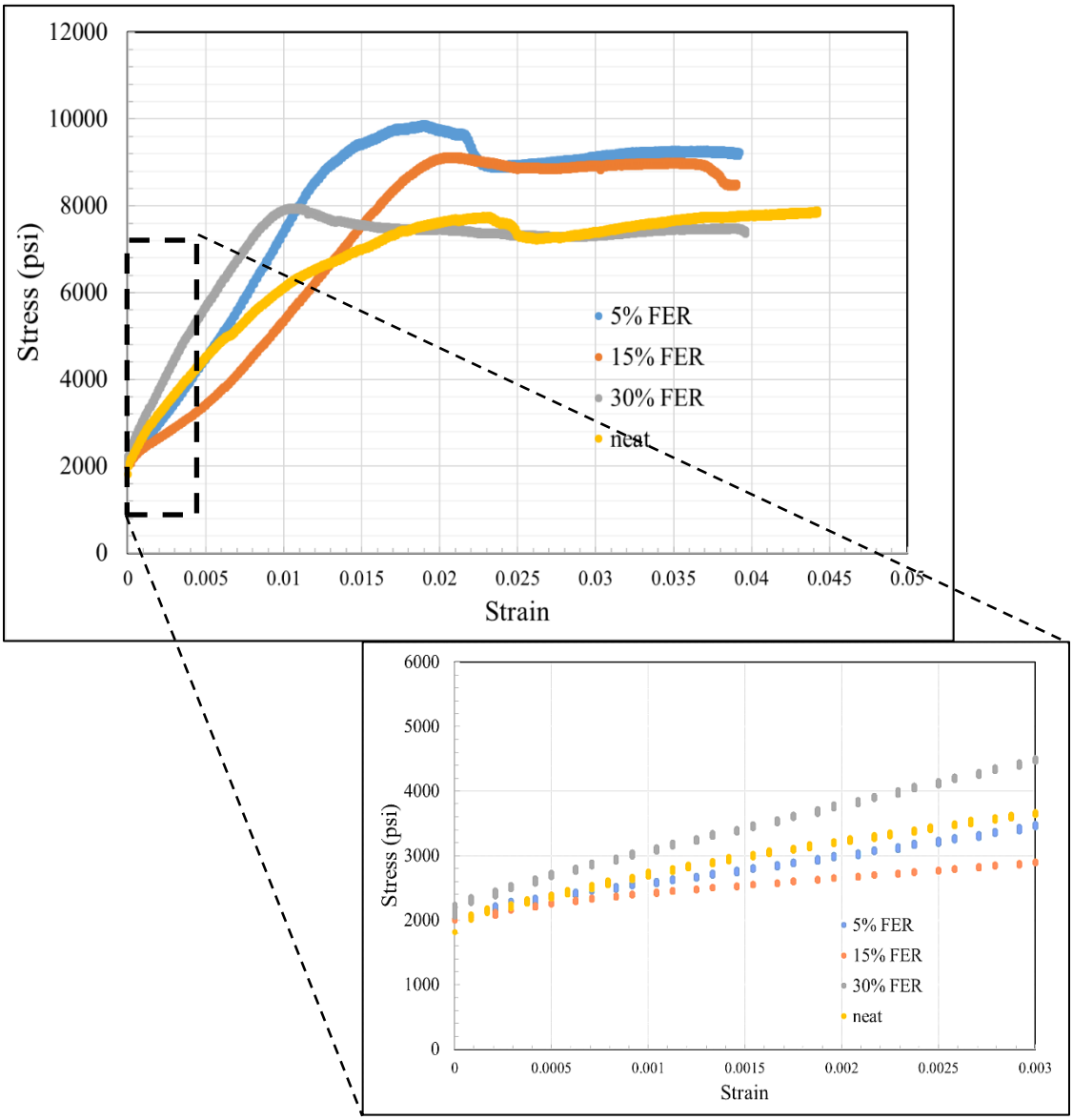

Fig-4.12. Triaxial test results for 5%, 15%, 30% FER added and neat class-H cement at 13.7M.Pa confining pressure and 90ºC. 5% FER added cement the highest axial stress at 68.8 MPa followed by 62.9 MPa and 54.5MPa for 15% and 30% additions respectively, while neat class-H cement sample had a maximum of 53.3 MPa. These results coincide with the UCS results showing a similar trend with 5% having the best performance. The initial linear regime is shown in a magnified scale in the inset and the slope of this initial linear regime is used to calculate the Young's modulus.

4.3 Petrophysical/hydraulic property testing:

Once the strength properties are tested, the last characterization that is required to conclude the suitability of the material for plugging and abandonment purposes is the petrophysical property testing. Zonal isolation is the most important factor for a material to be considered as a P&A solution. To measure this, we look at 2 very important properties namely porosity and permeability.

4.3.a. Porosity test:

Porosity is the percentage of the sample core that is filled with pore spaces or void spaces. This also has an impact on the material integrity as pore spaces could become initiation points for a fracture to begin under stress. This is measured using a porosimeter by taking a cement sample core in a matrix cup. The porosity is calculated based on the grain volume obtained from the combined gas law equation (P1V1= P2V2) where the gas pressure remains constant, and the volume is calculated from the gas that expands into the pore-spaces on applying that constant gas pressure. Another test that was done to study the porosity was the Mercury intrusion porosimetry (MIP). This was measured only for the best performer i.e., the 5% ferrierite added class-H cement to correlate it with the helium gas porosimetry measurements.

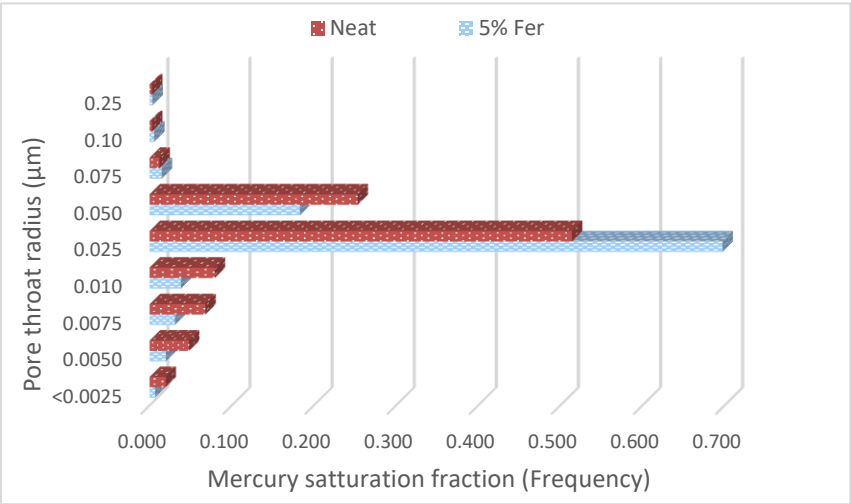

Fig-4.13. Pore throat radius as measured in mercury intrusion porosimetry where the most pore throat radius distribution is in the nano-range (0.025µm) supporting the hypothesis that

increase of porosity is attributed to the nano-porosity introduced by the addition of ferrierite. Ferrierite is a zeolite mineral that is characterized by crystalline structure with porosity in the nano-range and hence it could also support the fact that the porous crystalline structure of the zeolite is preserved in the cement matrix even after hydration.

4.3.b. Permeability test:

Permeability is a property that indicates the ability of a material to allow the passage of liquids or gases through it. This is measured using Darcy's law by measuring the flow rate while passing helium gas through a sample core at constant pressure. This is done under confining pressure to simulate downhole conditions to get a wholistic measurement of a simulated cement plug. As shown below in figure 4.12. is the porosity compared to the permeability values that were obtained for the 5%,15%, 30% ferrierite added cement samples in comparison to neat class-H cement.

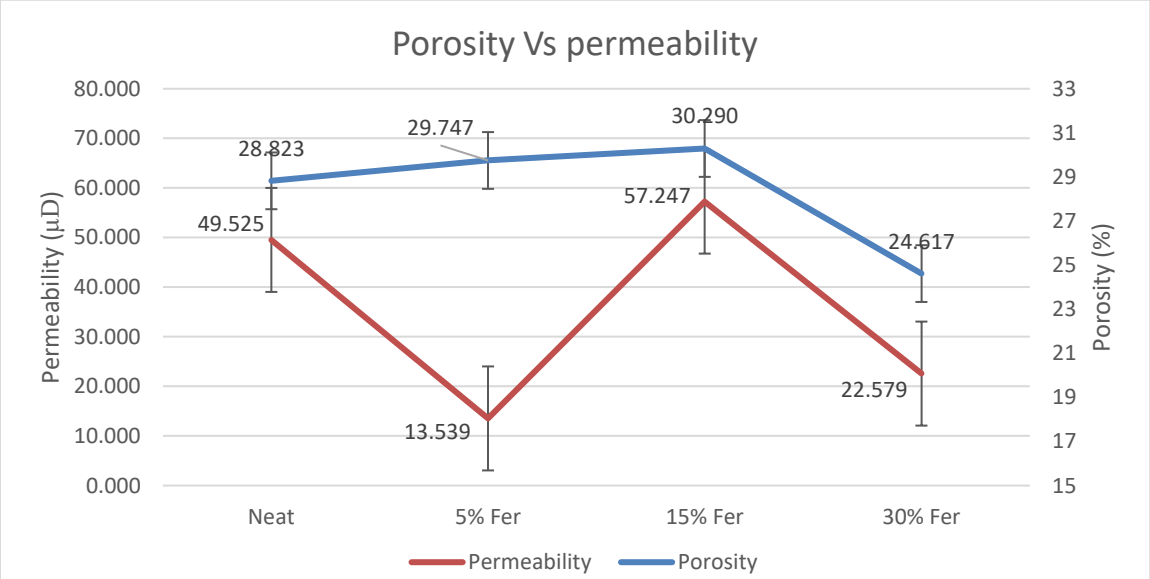

Fig-4.14. Average porosity and permeability values of 5%, 15%, 30% FER added, and Neat class-H cement measured using Corelab ultrapore 300 porosimeter and Nanoperm permeameter. (Vissa et al., GRC 2021, accepted manuscript) While 30% ferrierite has the least porosity due to better hydration, 5% ferrierite addition shows the best zonal isolation as it has the least permeability of 13.54 µD in copmparison to neat class-H cement (49.53 µD).

Porosity need not necessarily translate into permeability as the pore spaces could be isolated. Hence, permeability is also needed to be measured for the samples in order to get the complete petrophysical characterization. As observed in porosity measurements through helium gas expansion porosimetry, the addition of ferrierite slightly increased the porosity of the cement cores, but decreases for 30% which could be attributed to the enhanced hydration due to the stored pore water in ferrierite. Mercury intrusion porosimetry gives an insight into the distribution of the range of pore throat radii. Despite having a higher frequency of distribution in comparison to the neat cement, these pore throat sizes had been mostly distributed in the nanometer range and hence do not directly contribute to permeability. This could be noted in the permeability results. Hence, ferrierite addition does not impact the zonal isolation properties of the cement but apparently enhances it.

CHAPTER V

CONCLUSION

5.1. Discussion:

The SEM and EDS studies performed at the beginning had helped get an initial understanding of the chemical and morphological properties of zeolite. EDS shows an apparent change in atomic percentages of the zeolite, but the XRD shows phase stability which suggested the chemical stability of the material. Since EDS cannot be taken as a quantitative characterization technique on rough surfaces, it is used mostly to confirm the distribution of elements to make sure that the sample is zeolite. This comes in handy more in the EDS of cement to identify zeolites within the matrix and helps to show that the chemical make-up of the zeolites stays stable even after hydration. Also, XRD and EDS performed for plain zeolite dispersed in high-low pH solutions, as well as brine, DI water and oil show that there was no change in the phases of the zeolite in comparison to the plain control sample. The published literature with these results [9, 10] earlier as a part of this research, supports the hypothesis that the ferrierite is non-hydraulic and can act as a supplementary cementitious material that will not interfere with cement hydration directly but would provide morphological template for CSH. However further work needs to be performed to observe if zeolite shows late pozzolanic reaction and is responsible for self-healing. This is essential to support our hypothesis based on the earlier literature [46] that our research work was based on. Tests like Raman and XRF had also been performed to get the chemical characterization of these materials.

Raman spectroscopy showed that the peaks for ferrierite have been consistent in all the ferrierite added cement cores, indicating the stability of this mineral within hydrated cement matrix. The data shows that the ferrierite existed as a stable state in cement even after 28 days of curing at high temperature (90°C) and 95% RH (Relative humidity). XRF performed for unhydrated commercial geothermal zeolite cement and plain class-H cement show the ferrierite replacement and we could notice that it reduces the CaO content in the cement which is responsible for the more reactive phases in cement which tend to deteriorate on a longer run on exposure to harsh low – pH conditions. This shows that the ferrierite replacement by weight of cement could be advantageous to the end product but further testing was required to decide what percentage would be an ideal replacement for optimized hydration and enhanced strength and petrophysical properties.

The UCS data obtained comparing the 5%, 15%, and 30% ferrierite added cements, and neat class-H cement show a clear increase in the strength characteristics. It was observed that 5% Ferrierite added cement cores showing an average UCS of 9934.3 psi compared to neat class-H cement cores showing an average UCS of 7041psi. Based on this, a conclusion could be made that 5% ferrierite addition shows the best performance, also supporting the initial claim that zeolite addition improves the strength properties. It was noted that a similar trend was observed in Triaxial tests with 5% ferrierite addition showing superior performance with highest axial peak stress at 68.8 MPa compared to 53.3 MPa for neat class-H cement. Calculated young's modulus from triaxial tests had been observed to be reduced for 5% and 15% ferrierite additions compared to neat class-H but had increased for 30% ferrierite addition. Hardness and elastic modulus had also been higher for neat class-H cement compared to ferrierite added cements from indentation tests. Table-5.1 below gives us the average results of all the measured strength properties namely hardness and elastic modulus (indentation), Axial peak stress and elastic modulus (Triaxial), as well as compressive strength (unconfined compressive strength) as shown in the plots in the results section.

The complete raw data is provided in the appendix tables – 6.9 – 6.14.

	Indentation		Triaxial		UCS
	Hardness (Gpa)	EM (GPa) Ind	Axial peak stress (psi)	EM (GPa) triaxial	Comp. strength (psi)
Neat	0.506	15.72	7730	9.65	7041
5% Fer	0.394	14.03	9882	8.82	9934.3
15% Fer	0.319	11.006	9133	7.72	6652
30% Fer	0.256	7.88	7944	11.29	6319

Table-5.1 Summary of Mechanical tests for 16PPG Neat Class-H, 5%, 15%, and 30% ferrierite added class-H cement formulations

Porosity and permeability of the ferrierite added cements were measured along with that of neat class-H cement. While porosity did not differ much (Difference between 1-2%), Permeability showed a promising trend with 5% and 30% ferrierite added cements showing lower values (13.5 μD and 22.58 μD respectively) compared to neat class-H cement cores. Porosity was also found out to be in the nano-range with a pore throat radius distribution frequency mostly in the nanometer regime for the 5% ferrierite added sample as observed in mercury intrusion porosimetry. That was an interesting observation that would support the hypothesis that ferrierite added cement formulations show better petrophysical properties. Shown below is a schematic of the hypothesis.

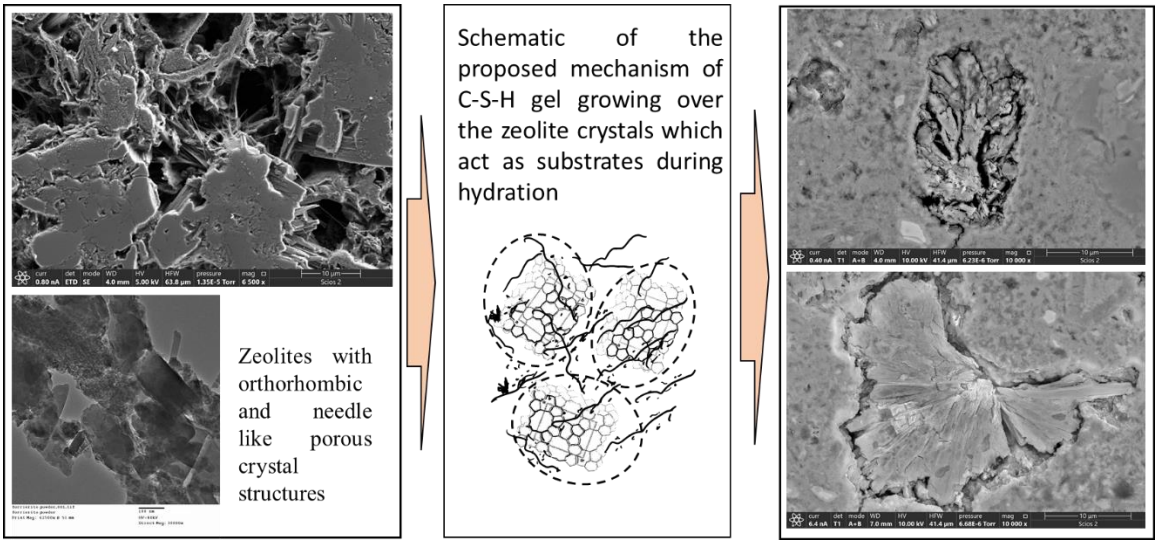

Fig-5.1. Schematic of proposed mechanism of zeolite in cement hydration with hydrated cement matrix seen around zeolite crystals in the final product while zeolite stays intact.

One very important observation from the literature was self-healing [46]. Though this study had not included an in-depth study for self-healing, we had observed morphological characteristics like the ones seen in earlier literature where self-healing was observed (Fig: 4.2 in results refer to figure 2.3 in literature survey). This is a very promising This shows that the zeolite that we had chosen for our studies is a good fit and would in the future help us create a robust barrier plugging material. However, a lot of research is yet to be done to understand the mechanism of these zeolite additions and it would be studied in our future work. The usage of tools like Raman, SEM and EDS analysis coupled with XRD would make a considerable addition to our research and are currently under progress. The integration of indentation and SEM as well as EDS is another future plan of work. Single-phase studies as well as experiments to determine self-healing capability would be designed for our future work. With all the current results which have been published and the ones under review, the planned future experiments for the research aim to understand the mechanism of the zeolite and its action in cement.

5.2. Conclusion:

The chemical stability of zeolites at elevated temperatures as well as subsurface and cement hydration conditions suggest that zeolite could act as a substrate for hydration without actively taking part in the reaction. While some literature suggests that zeolites interact with cement to form new phases[68, 103], there are many instances in our research where the zeolite phase was observed to be stable even after months of hydration. Cement samples containing 5% by weight of cement addition of ferrierite had shown a consistent improvement in UCS (41% increase compared to neat class-H) as well as possessed improved triaxial strength by 29% compared to neat class-H cement. Ferrierite XRD peaks obtained in hydrated cement suggest that ferrierite exhibits phase stability

within cement matrix and does not react with cement, like most pozzolanic materials used in cement-based composites [61, 62, 104]. Further work is required to understand the interaction between zeolite and cement and also how it is responsible for self-healing. Experiments like single phase studies and induced secondary hydration studies by curing the failed/fractured samples at high temperature conditions, need to be designed in future for observing the self-healing capability of this zeolite addition in cement. This is a very important reason for choosing this material as literature had strongly suggested self-healing with all the relevant observations [46]. Reproducing this same self-healing quality in wellbore cement for plugging and abandonment for repairing cracks and fractures would be a great improvement as zonal isolation is a must for this application. The literature strongly suggests the porous structure of zeolites hold a key to their exceptional behavior. Noted below, are the key insights from the research performed so far. The insights include conclusions supporting the hypothesis based on each of the following properties namely chemical, mechanical and petrophysical properties. Based on these observations, future work can be recommended.

5.2.1. Chemical and morphological properties:

As mentioned in the discussion, ferrierite can be concluded to be stable under harsh chemical conditions like high and low pH as well as at simulated downhole conditions (High temperature- 90°C). It does not show any interaction with water or brine or even organic materials making it ideal for our usage. Ferrierite remains as a stable phase even after cement hydration as the ferrierite crystal structure can still be noticed to remain in the cement matrix as observed in the following:

1) **Scanning electron microscopy:** SEM studies show that the crystalline morphological structure had been retained in zeolites even after exposure to sub-surface and hydration chemical

conditions. It had also been observed as a stable crystalline phase within a hydrated cement matrix.

2) **Energy dispersive X-Ray spectroscopy:** As observed in EDS, the chemical and elemental composition of ferrierite (Aluminosilicate) remained stable at reactive chemical conditions as well as post-hydration.

3) X-ray diffraction: This is the most promising result as the ferrierite phase had remained stable with prominent 2Ɵ peaks seen at 25.1951 and 25.5204 in hydrated 30% ferrierite added class-H as well as in the geothermal zeolite cement formulation. The best results were shown in the chemically treated ferrierite samples which had the same 2Ɵ peaks throughout at 9.2256, 23.5000, 25.1951 and 25.5204 characteristic of ferrierite-Mg. The only exception was an extra calcite peak that was observed at 29.4321 for ferrierite treated in $Ca(OH)_2$ which indicates the affinity of zeolites to calcium-based compounds.

4) **Raman spectroscopy:** This technique had also shown promising results with ferrierite as unreacted ferrierite phases were observed in each of the 5%, 15% and 30% ferrierite added samples at ~416nm. This was done using a 532nm excitation laser for all the samples so that the tests are uniform.

This would lead to our conclusion that ferrierite would enhance the properties of cement by acting as a scaffolding for hydration to take place enhancing the cement hydration and in turn improving the final properties of cement. This phase stability of ferrierite helps infer that characteristic pore structure of zeolites (Ferrierite in our studies) is being retained in the cement matrix. TEM was also used to observe the crystal structure of the zeolite for morphological characterization corresponding to the zeolite and was found to be similar to the structures observed in literature. The porous structure of zeolites is responsible for holding of pore water for secondary hydration and possible self-healing which need further conclusive studies. It can also improve the ion transport during hydration enhancing the overall hydration by acting as a substrate.

5.2.2. Mechanical properties:

Ferrierite addition had a significant effect on the mechanical strength properties as clearly observed in UCS and triaxial tests. There was a 41% increase in the UCS value for 5% by weight of cement ferrierite added to cement in comparison to the neat Class-H cement. Triaxial tests concluded the same with 5% ferrierite addition having a peak axial stress at 68.8MPa compared to that of neat at 53.2 MPa which is a 29% increase in comparison with neat class-H. Indentation tests also gave an average hardness (0.506GPa or 47.82 HV) and elastic modulus values of 15.72 GPa for neat class-H cement showing that it was a very brittle material. At 0.394GPa (37.3HV) hardness and 14.03GPA elastic modulus, 5% ferrierite added cores are slightly more ductile giving it the superior performance in UCS and Triaxial tests. Ferrierite addition was shown to lower the elastic modulus as seen in both indentation and triaxial testing. This indicates a more ductile nature of the resultant cement cores. An outlier was the elastic modulus value from the triaxial testing of 30% ferrierite added cement (11.29 GPa) which was higher than that of neat class-H cement core (9.65 GPa) which indicates the more brittle nature of the higher ferrierite addition. This could also mean that the hydration was highest in the 30% ferrierite added cement due to the increased water content showing the formation of more brittle cement phases. One more important fact that needs to be noted is that the triaxial test only gives localized stress-strain results and hence can only be good for calculating the average hardness and elastic modulus of the material. This cannot give the bulk elastic modulus as accurately as triaxial testing. Hence, triaxial test results are considered as a better evaluation of the material than indentation. From all these tests, it was also noted that 5% ferrierite addition had shown the best properties and hence can be recommended as an ideal formulation for P&A application.

5.2.3. Petrophysical/Hydraulic properties:

Porosity of the cement cores as measured by the helium gas porosimeter, was observed to increase with increase of Zeolite percentage up to 15% ferrierite addition (30.2% porosity compared to 28.82% for neat class-H) but drops for 30% addition (24.617%). This could be correlated to the increased water content in the cement slurry due to the water absorbed by the nano-pores observed in the crystal structure of ferrierite. This would be by means of capillary action when water is added to make the slurry. This increased water content could result in better hydration (as inferred from triaxial testing showing a more brittle nature for 30% ferrierite addition) and as a result, reduced pore spaces. The higher porosity of zeolite added cement could be explained by the nano-porosity observed in the zeolite crystal structure, as confirmed from the mercury intrusion porosimetry (MIP). This nano-porosity in the 0.025 μm range, does not translate into the effective cement porosity as the ferrierite nano-pores can be considered as isolated pore spaces. This can be confirmed by the low permeability that is observed for 5% Ferrierite added cement. Permeability was the lowest for 5% ferrierite added to the cement cores at 13.5 μD compared to 49.525 μD for neat class-H cement. Based on all these results and conclusions, 5% ferrierite addition could be considered as a recommended cement design for plugging and abandonment purposes. As 5% addition of ferrierite had shown the best zonal isolation properties as well as the best strength properties with more ductile nature compared to neat class-H cement.

Future work on this topic would be to investigate the mechanism behind the observed property enhancement. Desired properties like self-healing can also be tested by using techniques like flowthrough and CT to get a holistic understanding of the material. Also, further experiments like single-phase studies and curing the fractured samples at subsurface conditions need to be conducted to check the mechanism behind self-healing. Adapting this for cement formulations used for plugging and abandonment would be a breakthrough in P&A. Once self-healing is confirmed,

the research could concentrate on understanding how zeolite (ferrierite) interacts with cement in different stages by using highly advanced techniques like AFM, and FIB augmented SEM and EDS studies. EBSD could also be done on ion beam polished samples studying the interfacial phases at the grain boundaries further confirming whether the zeolite is stable post-hydration. A comparison between plain samples and self-healed samples can be done to observe whether zeolite acts as a sacrificial material by forming different phases determining the mechanism.

REFERENCES

1. EIA, U.S., *The Distribution of US Oil and Natural Gas Wells by Production Rate*. 2019.
2. Liu, H., et al. *Research and practice of full life cycle well integrity in HTHP well, Tarim Oilfield*. in *International Petroleum Technology Conference*. 2019. OnePetro.
3. Ahmed, S., S. Salehi, and C. Ezeakacha, *Review of gas migration and wellbore leakage in liner hanger dual barrier system: Challenges and implications for industry.* Journal of Natural Gas Science and Engineering, 2020. **78**: p. 103284.
4. Wang, H., Y. Ge, and L. Shi, *Technologies in deep and ultra-deep well drilling: Present status, challenges and future trend in the 13th Five-Year Plan period (2016–2020).* Natural Gas Industry B, 2017. **4**(5): p. 319-326.
5. Achang, M., L. Yanyao, and M. Radonjic, *A review of past, present, and future technologies for permanent plugging and abandonment of wellbores and restoration of subsurface geologic barriers.* Environmental Engineering Science, 2020. **37**(6): p. 395-408.
6. Calvert, D. and D.K. Smith. *Issues and techniques of plugging and abandonment of oil and gas wells*. in *SPE Annual Technical Conference and Exhibition*. 1994. Society of Petroleum Engineers.
7. Carroll, S., et al., *Review: Role of chemistry, mechanics, and transport on well integrity in CO2 storage environments.* International Journal of Greenhouse Gas Control, 2016. **49**: p. 149-160.
8. Salehi, S., et al., *Investigation of mix design and properties of geopolymers for application as wellbore cement.* Journal of Petroleum Science and Engineering, 2019. **178**: p. 133-139.
9. Vissa, S.V.K. and M. Radonjic. *Designing Wellbore Plugging and Abandonment Materials Based on Nature's Hydraulic Barrier Materials: A Solution to Prevent Hydrocarbon Leakage Over Time*. in *SPE International Conference and Exhibition on Health, Safety, Environment, and Sustainability*. 2020. Society of Petroleum Engineers.
10. Vissa, S.V.K., M. Radonjic, and Y. Li, *Sealing Wellbores at the end of their lifecycle to restore subsurface seal integrity and prevent offshore wellbore leakage.* Earth and Space Science Open Archive, 2019.

11. Herndon, J. and D.K. Smith, *Plugging wells for abandonment: a state-of-the-art study and recommended procedures*. 1976, Halliburton Services, Duncan, OK (USA).
12. Bullard, J.W., et al., *Mechanisms of cement hydration.* Cement and concrete research, 2011. **41**(12): p. 1208-1223.
13. El-Gamal, S.M.A., M.S. Amin, and M. Ramadan, *Hydration characteristics and compressive strength of hardened cement pastes containing nano-metakaolin.* HBRC Journal, 2019. **13**(1): p. 144-121.
14. Esteves, L.P., *On the hydration of water-entrained cement–silica systems: Combined SEM, XRD and thermal analysis in cement pastes.* Thermochimica Acta, 2011. **518**(1-2): p. 27-35.
15. Scrivener, K.L., P. Juilland, and P.J. Monteiro, *Advances in understanding hydration of Portland cement.* Cement and Concrete Research, 2015. **78**: p. 38-56.
16. Ylmén, R., et al., *Early hydration and setting of Portland cement monitored by IR, SEM and Vicat techniques.* Cement and Concrete Research, 2009. **39**(5): p. 433-439.
17. Naber, C., F. Bellmann, and J. Neubauer, *Influence of w/s ratio on alite dissolution and CSH precipitation rates during hydration.* Cement and Concrete Research, 2020. **134**: p. 106087.
18. Breul, P., J.-M. Geoffray, and Y. Haddani, *On-site concrete segregation estimation using image analysis.* Journal of Advanced Concrete Technology, 2008. **6**(1): p. 171-180.
19. El-Chabib, H. and M. Nehdi, *Effect of mixture design parameters on segregation of self-consolidating concrete.* ACI Materials Journal, 2006. **103**(5): p. 374.
20. Navarrete, I. and M. Lopez, *Understanding the relationship between the segregation of concrete and coarse aggregate density and size.* Construction and Building Materials, 2017. **149**: p. 741-748.
21. Panesar, D.K. and B. Shindman, *The effect of segregation on transport and durability properties of self consolidating concrete.* Cement and Concrete Research, 2012. **42**(2): p. 252-264.
22. Artioli, G., et al., *Nanoseeds as modifiers of the cement hydration kinetics*, in *Smart Nanoconcretes and Cement-Based Materials*. 2020, Elsevier. p. 257-269.
23. Canpolat, F., et al., *Use of zeolite, coal bottom ash and fly ash as replacement materials in cement production.* Cement and Concrete Research, 2004. **34**(5): p. 731-735.
24. Franus, W., R. Panek, and M. Wdowin. *SEM investigation of microstructures in hydration products of portland cement*. in *2nd International Multidisciplinary Microscopy and Microanalysis Congress*. 2015. Springer.
25. Juenger, M.C.G. and R. Siddique, *Recent advances in understanding the role of supplementary cementitious materials in concrete.* Cement and Concrete Research, 2015. **78**: p. 71-80.
26. John, E., T. Matschei, and D. Stephan, *Nucleation seeding with calcium silicate hydrate–A review.* Cement and Concrete Research, 2018. **113**: p. 74-85.

27. Chollet, M. and M. Horgnies, *Analyses of the surfaces of concrete by Raman and FT-IR spectroscopies: comparative study of hardened samples after demoulding and after organic post-treatment.* Surface and Interface Analysis, 2011. **43**(3): p. 714-725.
28. de la Cruz, J.C., J.M. del Campo, and D. Colorado. *A Much Better Concrete with Zeolite Additions-State of the Art Review*. in *2nd International Conference on Emerging Trends in Engineering and Technology*. 2014.
29. Dembovska, L., et al., *Effect of Pozzolanic Additives on the Strength Development of High Performance Concrete.* Procedia Engineering, 2017. **172**: p. 202-210.
30. Diamond, S., *The microstructure of cement paste and concrete—a visual primer.* Cement and Concrete Composites, 2004. **26**(8): p. 919-933.
31. Emam, E. and S. Yehia, *Performance of concrete containing zeolite as a supplementary cementitious material.* Int. Res. J. Eng. Technol, 2017: p. 1619-1625.
32. Feng, N.-Q., G.-Z. Li, and X.-W. Zang, *High-strength and flowing concrete with a zeolitic mineral admixture.* Cement, concrete and aggregates, 1990. **12**(2): p. 61-69.
33. Halstead, W.J., *Use of fly ash in concrete.* NCHRP Synthesis of Highway Practice, 1986(127).
34. Askarinejad, S. and N. Rahbar, *Effects of Cement–Polymer Interface Properties on Mechanical Response of Fiber-Reinforced Cement Composites.* Journal of Nanomechanics and Micromechanics, 2017. **7**(2).
35. Barbuta, M., M. Rujanu, and A. Nicuta, *Characterization of Polymer Concrete with Different Wastes Additions.* Procedia Technology, 2016. **22**: p. 407-412.
36. Le, H.T., et al., *The mix design for self-compacting high performance concrete containing various mineral admixtures.* Materials & Design, 2015. **72**: p. 51-62.
37. Brady, S., et al. *Recent technological advances help solve cement placement problems in the Gulf of Mexico*. in *SPE/IADC Drilling Conference*. 1992. Society of Petroleum Engineers.
38. Denney, D., *More-effective plug-and-abandonment cementing technique.* Journal of Petroleum Technology, 2012. **64**(05): p. 132-135.
39. Desai, P.C., S. Hekelaar, and L. Abshire. *Offshore Well Plugging and Abandonment: Challenges and Technical Solutions*. in *Offshore Technology Conference*. 2013. Offshore Technology Conference.
40. Ferg, T.E., et al. *Novel approach to more effective plug and abandonment cementing techniques*. in *SPE Arctic and extreme environments conference and exhibition*. 2011. Society of Petroleum Engineers.
41. Dusseault, M.B., R.E. Jackson, and D. Macdonald, *Towards a road map for mitigating the rates and occurrences of long-term wellbore leakage*. 2014: University of Waterloo Waterloo, ON, Canada.
42. Khalifeh, M. and A. Saasen, *Introduction to Permanent Plug and Abandonment of Wells*. 2020: Springer Nature.
43. Bachu, S. and D.B. Bennion, *Experimental assessment of brine and/or CO2 leakage through well cements at reservoir conditions.* International Journal of Greenhouse Gas Control, 2009. **3**(4): p. 494-501.

44. Zhang, M. and S. Bachu, *Review of integrity of existing wells in relation to CO2 geological storage: What do we know?* International Journal of Greenhouse Gas Control, 2011. **5**(4): p. 826-840.
45. Ahn, T.-H. and T. Kishi, *Crack self-healing behavior of cementitious composites incorporating various mineral admixtures.* Journal of Advanced Concrete Technology, 2010. **8**(2): p. 171-186.
46. Pyatina, T., et al., *Self-repairing properties of OPC clinker/natural zeolite blend in water and alkali carbonate environments at 270°C.* Advances in Cement Research, 2018. **30**(1): p. 8-23.
47. Liu, X., et al. *True self-healing geopolymer cements for improved zonal isolation and well abandonment*. in *SPE/IADC Drilling Conference and Exhibition*. 2017. Society of Petroleum Engineers.
48. Su, Y.-F., et al., *Autogenous healing performance of internal curing agent-based self-healing cementitious composite.* Cement and Concrete Composites, 2020. **114**: p. 103825.
49. Vrålstad, T., et al., *Plug & abandonment of offshore wells: Ensuring long-term well integrity and cost-efficiency.* Journal of Petroleum Science and Engineering, 2019. **173**: p. 478-491.
50. Liteanu, E., C.J. Spiers, and C.J. Peach, *Failure behaviour wellbore cement in the presence of water and supercritical CO2.* Energy Procedia, 2009. **1**(1): p. 3553-3560.
51. Kiran, R., et al., *Identification and evaluation of well integrity and causes of failure of well integrity barriers (A review).* Journal of Natural Gas Science and Engineering, 2017. **45**: p. 511-526.
52. Skorpa, R. and T. Vrålstad, *Leakages Through Radial Cracks in Cement Sheaths: Effect of Geometry, Viscosity, and Aperture.* Journal of Energy Resources Technology, 2021. **144**(1).
53. Nygaard, R., et al., *Effect of dynamic loading on wellbore leakage for the wabamun area CO2-sequestration project.* Journal of Canadian Petroleum Technology, 2014. **53**(01): p. 69-82.
54. Mindess, S., F. Young, and D. Darwin, *Concrete 2nd Editio.* Technical Documents, 2003.
55. Materials, A.S.o.T.a., *Standard Specification for Air-Entraining Admixtures for Concrete*, in *ASTM C260/C260M-10a(2016)*. 2016.
56. Materials, A.S.o.T.a., *Mineral Admixtures*, in *STP169A-EB*. 1965.
57. Mehdipour, I. and K.H. Khayat, *Elucidating the role of supplementary cementitious materials on shrinkage and restrained-shrinkage cracking of flowable eco-concrete.* Journal of Materials in Civil Engineering, 2018. **30**(3): p. 04017308.
58. Rakhimova, N.R. and R.Z. Rakhimov, *Literature Review of Advances in Materials Used in Development of Alkali-Activated Mortars, Concretes, and Composites.* Journal of Materials in Civil Engineering, 2019. **31**(11): p. 03119002.
59. Scrivener, K.L. and R.J. Kirkpatrick, *Innovation in use and research on cementitious material.* Cement and concrete research, 2008. **38**(2): p. 128-136.

60. Liu, J., et al., *The effect of SCMs and SAP on the autogenous shrinkage and hydration process of RPC.* Construction and Building Materials, 2017. **155**: p. 239-249.
61. Deboucha, W., et al., *Natural pozzolana addition effect on compressive strength and capillary water absorption of Mortar.* Energy Procedia, 2017. **139**: p. 689-695.
62. Isaia, G.C., A.L.G. Gastaldini, and R. Moraes, *Physical and pozzolanic action of mineral additions on the mechanical strength of high-performance concrete.* Cement and concrete composites, 2003. **25**(1): p. 69-76.
63. Brooks, J. and M.M. Johari, *Effect of metakaolin on creep and shrinkage of concrete.* Cement and concrete composites, 2001. **23**(6): p. 495-502.
64. Wild, S., J.M. Khatib, and A. Jones, *Relative strength, pozzolanic activity and cement hydration in superplasticised metakaolin concrete.* Cement and concrete research, 1996. **26**(10): p. 1537-1544.
65. Sabir, B.B., S. Wild, and J. Bai, *Metakaolin and calcined clays as pozzolans for concrete: a review.* Cement and Concrete Composites, 2001. **23**(6): p. 441-454.
66. Massazza, F., *Pozzolanic cements.* Cement and Concrete composites, 1993. **15**(4): p. 185-214.
67. Mohamed, M.R. and H.A. Mohamed, *Mechanical strength and corrosion detection of pozzolanic cement.* HBRC Journal, 2019. **9**(2): p. 103-108.
68. Uzal, B., et al., *Pozzolanic activity of clinoptilolite: a comparative study with silica fume, fly ash and a non-zeolitic natural pozzolan.* Cement and Concrete Research, 2010. **40**(3): p. 398-404.
69. Jana, D. *A new look to an old pozzolan, clinoptilolite–a promising pozzolan in concrete*. in *Proceedings of the 29th ICMA conference on cement microscopy*. 2007. Curran Associates Inc Quebec City.
70. Siddique, R. and D. Kaur, *Properties of concrete containing ground granulated blast furnace slag (GGBFS) at elevated temperatures.* Journal of Advanced Research, 2012. **3**(1): p. 45-51.
71. Mueller, D.T., et al. *Portland cement-blast furnace slag blends in oilwell cementing applications*. in *SPE Annual Technical Conference and Exhibition*. 1995. Society of Petroleum Engineers.
72. Abdel Rahman, A., et al., *Characteristics of Portland blast-furnace slag cement containing cement kiln dust and active silica.* Arabian Journal of Chemistry, 2016. **9**: p. S138-S143.
73. Wang, S.-D. and K.L. Scrivener, *Hydration products of alkali activated slag cement.* Cement and Concrete Research, 1995. **25**(3): p. 561-571.
74. Luke, K. and F.P. Glasser, *Selective dissolution of hydrated blast furnace slag cements.* Cement and Concrete Research, 1987. **17**(2): p. 273-282.
75. Sugama, T., L.E. Brothers, and T.R.V.d. Putte, *Acid-resistant cements for geothermal wells: sodium silicate activated slag/fly ash blends.* Advances in Cement Research, 2005. **17**(2): p. 65-75.
76. Özbay, E., M. Erdemir, and H.İ. Durmuş, *Utilization and efficiency of ground granulated blast furnace slag on concrete properties–A review.* Construction and Building Materials, 2016. **105**: p. 423-434.

77. Palou, M.T., et al., *Blended cements consisting of Portland cement–slag–silica fume–metakaolin system.* Journal of Thermal Analysis and Calorimetry, 2016. **125**(3): p. 1025-1034.
78. Deboucha, W., et al., *Effect of Incorporating Blast Furnace Slag and Natural Pozzolana on Compressive Strength and Capillary Water Absorption of Concrete.* Procedia Engineering, 2015. **108**: p. 254-261.
79. Li, G., *Properties of high-volume fly ash concrete incorporating nano-SiO2.* Cement and Concrete research, 2004. **34**(6): p. 1043-1049.
80. Bijen, J., *Benefits of slag and fly ash.* Construction and Building Materials, 1996. **10**(5): p. 309-314.
81. Chindaprasirt, P., C. Jaturapitakkul, and T. Sinsiri, *Effect of fly ash fineness on compressive strength and pore size of blended cement paste.* Cement and Concrete Composites, 2005. **27**(4): p. 425-428.
82. Langan, B.W., K. Weng, and M.A. Ward, *Effect of silica fume and fly ash on heat of hydration of Portland cement.* Cement and Concrete Research, 2002. **32**(7): p. 1045-1051.
83. Srivastava, V., et al., *Effect of silica fume on workability and compressive strength of OPC concrete.* Journal of Environment and Nanotechnology, 2014. **3**(3): p. 32-35.
84. Nili, M. and A. Ehsani, *Investigating the effect of the cement paste and transition zone on strength development of concrete containing nanosilica and silica fume.* Materials & Design, 2015. **75**: p. 174-183.
85. Valipour, M., et al., *Comparing a natural pozzolan, zeolite, to metakaolin and silica fume in terms of their effect on the durability characteristics of concrete: A laboratory study.* Construction and Building Materials, 2013. **41**: p. 879-888.
86. Sičáková, A., et al., *Long-term properties of cement-based composites incorporating natural zeolite as a feature of progressive building material.* Advances in Materials Science and Engineering, 2017. **2017**.
87. Poon, C., et al., *A study on the hydration rate of natural zeolite blended cement pastes.* Construction and Building Materials, 1999. **13**(8): p. 427-432.
88. Ahmadi, B. and M. Shekarchi, *Use of natural zeolite as a supplementary cementitious material.* Cement and Concrete Composites, 2010. **32**(2): p. 134-141.
89. Chen, J., et al., *Effects of superfine zeolite on strength, flowability and cohesiveness of cementitious paste.* Cement and Concrete Composites, 2017. **83**: p. 101-110.
90. Ramezanianpour, A.A., et al., *Micro and macro level properties of natural zeolite contained concretes.* Construction and Building Materials, 2015. **101**: p. 347-358.
91. Taylor, J. and L. Aldridge, *Full-profile Rietveld quantitative XRD analysis of Portland cement: Standard XRD profiles for the major phase tricalcium silicate (C3S: 3CaO. SiO2).* Powder Diffraction, 1993. **8**(3): p. 138-144.
92. BENSTED, J., *Uses of Raman Spectroscopy in Cement Chemistry.* Journal of the American Ceramic Society, 1976. **59**(3-4): p. 140-143.

93. Black, L., et al., *Hydration of tricalcium aluminate (C 3 A) in the presence and absence of gypsum—studied by Raman spectroscopy and X-ray diffraction.* Journal of Materials Chemistry, 2006. **16**(13): p. 1263-1272.
94. Black, L., et al., *In situ Raman analysis of hydrating C3A and C4AF pastes in presence and absence of sulphate.* Advances in applied ceramics, 2006. **105**(4): p. 209-216.
95. Conjeaud, M. and H. Boyer, *Some possibilities of Raman microprobe in cement chemistry.* Cement and Concrete Research, 1980. **10**(1): p. 61-70.
96. Garg, N. and K. Wang, *Applying raman spectroscopy for studying cement-based materials.* 2012.
97. Richardson, I., et al., *Characterisation of cement hydrate phases by TEM, NMR and Raman spectroscopy.* Advances in Cement Research, 2010. **22**(4): p. 233-248.
98. Babikian, S.H., *Raw Materials Analysis by XRF in the Cement Industry.* Advances in X-ray Analysis, 1992. **36**: p. 139-144.
99. Bulychev, S., et al., *Determination of Young modulus by the hardness indentation diagram.* Zavodskaya Laboratoriya, 1975. **41**(9): p. 1137-1140.
100. materials, A.s.o.t.a., *Standard Test Methods for Compressive Strength of Molded Soil-Cement Cylinders*, in *D1633-17*. 2018.
101. materials, A.S.o.t.a., *Standard Test Method for Compressive Strength of Cylindrical Concrete Specimens*, in *C39/C39M − 21*. 2021.
102. Ma, Z., R.P. Gamage, and C. Zhang, *Application of nanoindentation technology in rocks: a review.* Geomechanics and Geophysics for Geo-Energy and Geo-Resources, 2020. **6**(4): p. 1-27.
103. Snellings, R., et al., *Early age hydration and pozzolanic reaction in natural zeolite blended cements: Reaction kinetics and products by in situ synchrotron X-ray powder diffraction.* Cement and Concrete Research, 2010. **40**(12): p. 1704-1713.
104. Caputo, D., B. Liguori, and C. Colella, *Some advances in understanding the pozzolanic activity of zeolites: The effect of zeolite structure.* Cement and Concrete Composites, 2008. **30**(5): p. 455-462.

APPENDICES

1) EDS Elemental analysis:

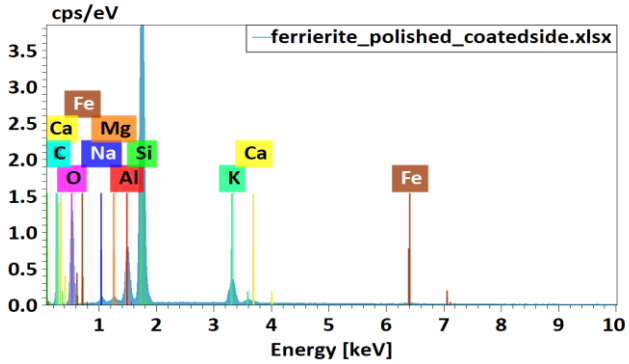

Fig 6.1. EDS chart for Ferrierite with counts plotted against energy (KeV) showing the elements that are present in the matertial

Element	At. No.	Mass [%]	Mass Norm. [%]	Atom [%]
Carbon	6	31.51	26.22	37.47
Oxygen	8	46.62	38.80	41.63
Sodium	11	0.91	0.76	0.57
Magnesium	12	0.50	0.42	0.29
Aluminium	13	6.05	5.04	3.21
Silicon	14	29.79	24.79	15.15
Potassium	19	3.96	3.30	1.45
Calcium	20	0.34	0.28	0.12
Iron	26	0.46	0.38	0.12
		120.15	100	100

Table-6.1 Atomic percentages of the different elements present in Ferrierite giving its elemental composition.

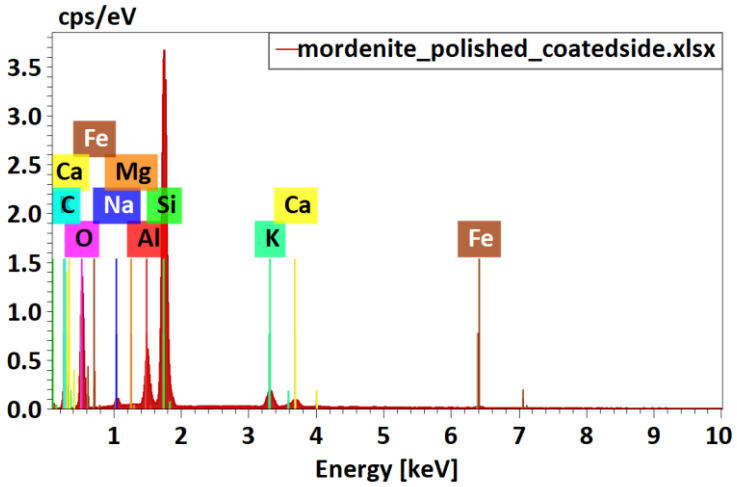

Fig 6.2. EDS chart for Mordenite (2nd prospective zeolite) with counts plotted against energy (KeV)

Element	At. No.	Mass [%]	Mass Norm. [%]	Atom [%]
Carbon	6	36.12	28.41	39.31
Oxygen	8	52.88	41.60	43.21
Sodium	11	1.27	1.00	0.72
Magnesium	12	0.06	0.05	0.03
Aluminium	13	5.13	4.04	2.49
Silicon	14	28.16	22.15	13.11
Potassium	19	2.09	1.64	0.70
Calcium	20	1.10	0.87	0.36
Iron	26	0.31	0.24	0.07
		127.12	100	100

Table-6.2. Atomic percentages of the different elements present in Mordenite giving the elemental composition.

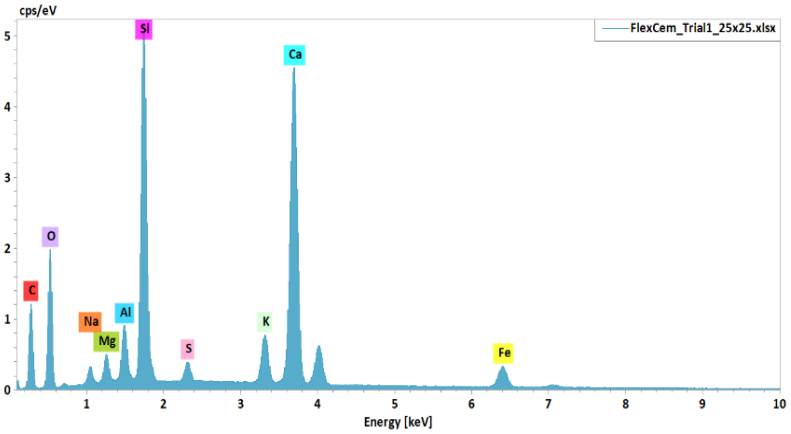

Fig 6.3. EDS chart for commercial geothermal zeolite cement with counts plotted against energy (KeV)

Element	At. No.	Mass [%]	Mass Norm. [%]	Atom [%]
Carbon	6	21.09557	20.993	33.86686
Oxygen	8	34.22856	34.06215	41.25226
Sodium	11	1.031433	1.026418	0.865106
Magnesium	12	1.150745	1.14515	0.912948
Aluminium	13	2.09514	2.084954	1.497302
Silicon	14	11.27057	11.21577	7.737959
Sulfur	16	0.797065	0.79319	0.479305
Potassium	19	2.630493	2.617704	1.297305
Calcium	20	22.44085	22.33175	10.79683
Iron	26	3.74813	3.729908	1.294129
		100.4885	100	100

Table-6.3 Atomic percentages of various elements present in commercial geothermal zeolite cement giving the elemental composition.

		Fer. Control	Fer.Ca(OH)2	Fer.HCl	Fer.NaCl	Fer. Oil	Fer. Water
Element	At. Number	Atom%	Atom%	Atom%	Atom%	Atom%	Atom%
Oxygen	8	65.69	41.57	63.32	58.72	64.03	60.30
Sodium	11	1.1	0.10	0.01	2.46	1.13	1.06
Magnesium	12	0.72	0.36	0.28	0.49	0.56	0.46
Aluminium	13	5.37	2.20	2.70	4.68	4.34	4.71
Silicon	14	24.43	19.54	33.36	30.95	26.60	30.08
Potassium	19	2.04	0.06	0.31	1.86	2.19	2.57
Calcium	20	0.45	35.72	0.00	0.00	0.23	0.17
Iron	26	0.21	0.45	0.01	0.83	0.93	0.64

Table-6.4 Consolidated atomic percentages of various elements for ferrierite in different chemical conditions (Plots)-(Figures 4.1 g&h). This elemental distribution is acquired from EDS and can be used as a chemical characterization technique which could be used to predict the predominant chemical phases in the material based on the elemental composition. For example and increased elemental percentage of aluminum and silicon in a particular region could indicate the presence of zeolite.

2) XRD data analysis:

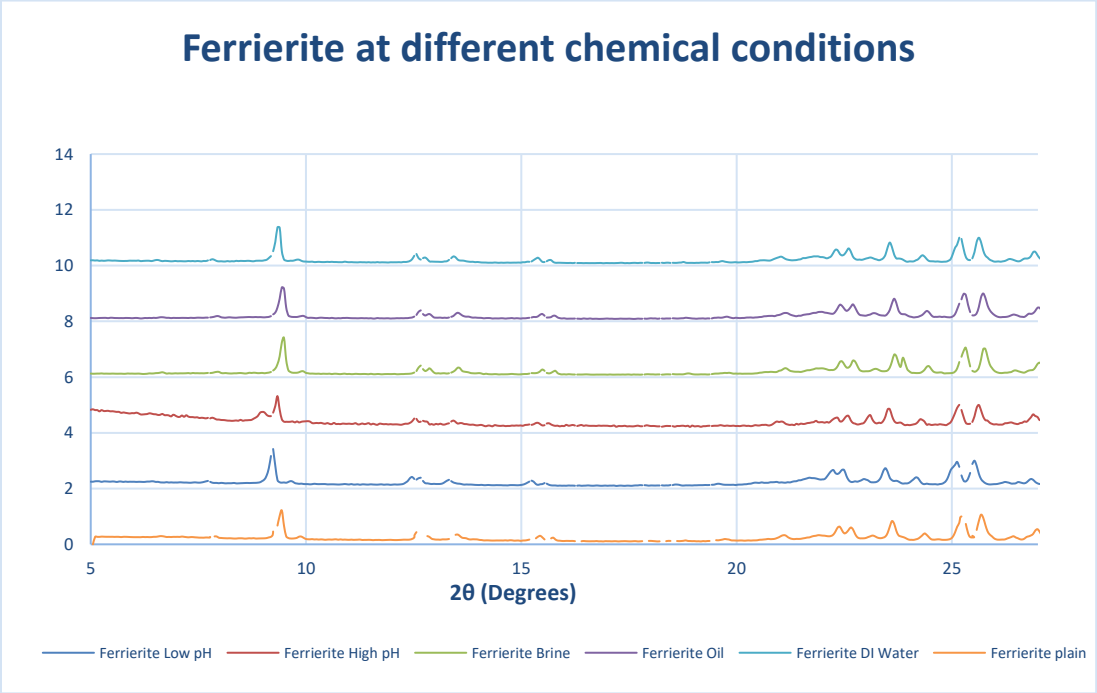

Fig 6.4. Consolidated XRD for ferrierite exposed to different chemical conditions Link this was one of the first tests performed to establish the chemical and phase stability of ferrierite and had formed the basis for our initial hypothesis.

3) Raman spectroscopy information for the plots obtained:

Neat Class-H cement	**5% Fer added Cement**	**15% Fer added cement**	**30% Fer added cement**
UHTS300S_GREEN _NIR: Excitation Wavelength [nm]: 532.262 Laser Power [mW]: 5.000 Grating: G2: 600 g/mm BLZ=500nm Center Wavelength [nm]: 594.993 Spectral Center [rel. 1/cm]: 1980.823	UHTS300S_GREEN _NIR: Excitation Wavelength [nm]: 532.262 Laser Power [mW]: 4.967 Grating: G2: 600 g/mm BLZ=500nm Center Wavelength [nm]: 594.993 Spectral Center [rel. 1/cm]: 1980.823	UHTS300S_GREEN _NIR: Excitation Wavelength [nm]: 532.262 Laser Power [mW]: 4.965 Grating: G2: 600 g/mm BLZ=500nm Center Wavelength [nm]: 594.993 Spectral Center [rel. 1/cm]: 1980.823	UHTS300S_GREEN _NIR: Excitation Wavelength [nm]: 532.262 Laser Power [mW]: 4.960 Grating: G2: 600 g/mm BLZ=500nm Center Wavelength [nm]: 594.993 Spectral Center [rel. 1/cm]: 1980.823

Sample Location (global position): Position X [µm]: 484.975 Position Y [µm]: -3509.300 Position Z [µm]: 98.720	Sample Location (global position): Position X [µm]: 5092.425 Position Y [µm]: -7015.400 Position Z [µm]: -0.960 (Live Auto Focus)	Sample Location (global position): Position X [µm]: 5478.875 Position Y [µm]: -7395.750 Position Z [µm]: -25.000	Sample Location (global position): Position X [µm]: 6485.325 Position Y [µm]: -7995.175 Position Z [µm]: -26.180
Large Scale Image: Scan Origin X [µm]: 0.000 Scan Origin Y [µm]: 0.000 Scan Origin Z [µm]: Live Auto Focus	Large Scale Image: Scan Origin X [µm]: 4197.380 Scan Origin Y [µm]: -7050.100 Scan Origin Z [µm]: Live Auto Focus	Large Scale Image: Scan Origin X [µm]: 5478.880 Scan Origin Y [µm]: -7395.750 Scan Origin Z [µm]: Live Auto Focus	Large Scale Image: Scan Origin X [µm]: 6485.330 Scan Origin Y [µm]: -7995.170 Scan Origin Z [µm]: Live Auto Focus

Table-6.5 Information for Raman parameters used for acquiring the data.

Note: Integration time and number of accumulations and power were kept nearly constant for all the samples to ensure uniformity.

General information:
DR316B_LD,DD:
Width [Pixels]: 2000
Height [Pixels]: 256
Temperature [°C]: -59
Cycle Time [s]: 0.58191
Camera Serial Nr.: 7349
AD Converters: AD1 (16Bit)
Vertical Shift Speed [µs]: 32.13
Horizontal Shift Speed [MHz]: 0.13
Preamplifier Gain: 4
ReadMode: Single Track (Row 8 -> 16)

Number Of Accumulations: 30
Integration Time [s]: 1.00000

Objective Name: Zeiss EC Epiplan-Neofluar Dic 50x / 0.8
Objective Magnification: 50.0

Large area scan information:

Scan (Area):
Points per Line: 100
Lines per Image: 100
Scan Width [µm]: 1000.000
Scan Height [µm]: 1000.000
Focus

Gamma [°]: 0.000
Scan Speed [s/Line]: 10.000
Integration Time [s]: 0.1

4) XRF Data :

Oxide:	Net	Wt%	At%	I-Error%	BG	Wt-Error
Al2O3	788.0901	6.47	4.06	0.81	13.6	0.05
SiO2	6501	29.65	31.52	0.28	28.75	0.09
SO3	3539.45	9.48	7.57	0.38	45.65	0.04
K2O	1726.355	1.81	1.23	0.55	23.7	0.01
CaO	47520.8	46.27	52.7	0.1	26.85	0.07
TiO2	492.75	0.52	0.42	1.01	3.6	0.01
MnO	792.95	0.26	0.24	0.8	8.55	0
Fe2O3	18683.75	5.31	2.12	0.16	23.55	0.01
ZnO	432.85	0.06	0.04	1.08	3.6	0
SrO	2539.9	0.17	0.1	0.45	7.95	0
Total		100	100			
kV	50		Live Tm	20		
uA	1000		Reso	157		
Itera.	3		Method	FP-NoStds		

Table-6.6 XRF data for commercial geothermal zeolite cement cement showing the various oxides present in it and their weight percentages, atomic percentages.

Oxide:	Net	Wt%	At%	I-Error%	BG	Wt-Error
Al2O3	172.5187	1.47	0.88	1.86	16.6	0.03
SiO2	3719.2	16.28	16.55	0.37	32.3	0.06
SO3	3090.2	6.97	5.31	0.41	48.8	0.03
K2O	598.3967	0.53	0.34	0.95	22.1	0.01
CaO	76896.8	68.08	74.13	0.08	25.7	0.09
TiO2	177.35	0.23	0.17	1.71	2.9	0
MnO	239.9	0.1	0.08	1.49	8.1	0
Fe2O3	17256.15	5.93	2.27	0.17	19.65	0.01
ZnO	878.1	0.14	0.1	0.76	4.8	0
SrO	3420.9	0.28	0.16	0.38	9.9	0
Total		100	100			
kV	50		Live Tm	20		
uA	1000		Reso	157		

Itera.	3		Method	FP-NoStds		

Table-6.7 XRF data for Neat Class-H cement showing the various oxides present in it and their weight percentages, atomic percentages.

Oxide:	Net	Wt%	At%	I-Error%	BG	Wt-Error
Al2O3	1052.852	8.16	5.16	0.69	6.3	0.06
SiO2	17443.65	82.43	88.41	0.17	6.3	0.16
K2O	4093.999	6.05	4.14	0.35	22.05	0.02
CaO	887.1	1.12	1.29	0.76	15.6	0.01
TiO2	200.75	0.13	0.11	1.62	4.8	0
MnO	62.3	0.01	0.01	3.14	7.2	0
Fe2O3	10730.8	1.81	0.73	0.22	15	0
SrO	1724.1	0.06	0.04	0.54	5.9	0
RhO	2032.6	0.22	0.12	0.5	16.5	0
Total		100	100			
kV	50		Live Tm	20		
uA	1000		Reso	157		
Itera.	4		Method	FP-NoStds		

Table-6.8 XRF data for Ferrierite showing the various oxides present in the zeolite and their weight percentages, atomic percentages.

5) Indentation data:

	Hardness average (Gpa)	EM average (GPa)
Neat	0.506	15.72
5% Fer	0.394	14.03
15% Fer	0.319	11.01
30% Fer	0.256	7.88

Table-6.9 Average indentation data.

Test	X	Y	Max Load	Max Depth	Hardness(GPa)	Hardness(HV)	Modulus	Martens
Test 1	0.000119	-0.00013	4950.274	21835.83	0.505586771	47.77542192	16.64911477	0.392819008
Test 2	0.400181	0.000129	4950.274	21148.34	0.563844522	53.28048809	14.59690866	0.418773781

Test 3	0.800073	0.000387	4953.632	22111.27	0.480605822	45.41484719	18.75281674	0.383353225
Test 4	1.200006	0.000695	4947.588	24048.45	0.410629926	38.80247489	14.75382792	0.323684722
Test 5	1.599919	0.000943	4944.901	24552.85	0.395838826	37.40478989	13.73453127	0.310353387
Test 6	-0.00014	-0.39876	4944.901	21717.5	0.5360446	50.65353444	13.62805034	0.396680304
Test 7	0.399982	-0.39844	4958.333	21490.9	0.534303816	50.48903913	15.56231253	0.406189968
Test 8	0.799845	-0.39817	4938.857	22537.65	0.46571813	44.00803466	16.99891534	0.367884957
Test 9	1.199788	-0.39794	4950.274	20592.45	0.570429414	53.90272746	18.44356591	0.441688276
Test 10	1.599681	-0.39767	4932.813	23371.06	0.425849966	40.24069255	17.30009703	0.341696691
Test 11	-0.00035	-0.79743	4961.02	22697.32	0.5360446	44.92197674	14.45292838	0.364354747
Test 12	0.399734	-0.79709	4954.304	23204.39	0.534303816	41.60817506	16.15242479	0.348132889
Test 13	0.799617	-0.79677	4965.049	20976.28	0.46571813	51.87903527	18.20220955	0.426942568
Test 14	1.199559	-0.79641	4944.23	21878.73	0.570429414	47.51069756	16.59625881	0.390802565
Test 15	1.599442	-0.79603	4942.215	24177.88	0.425849966	39.55806266	12.49545767	0.319880712
Test 16	-0.00063	-1.1957	4947.588	22628.1	0.47998532	45.35621285	14.10373195	0.365594848
Test 17	0.399466	-1.19534	4940.2	22930.54	0.475957607	44.97561403	12.63516302	0.355482969
Test 18	0.799359	-1.19504	4946.916	20285.92	0.62232352	58.806461	14.9647498	0.454828876
Test 19	1.199272	-1.19471	4948.259	18851.66	0.707457216	66.85116962	18.61619791	0.526812624

Test 20	1.599125	-1.19439	4946.916	23179.57	0.432701703	40.88814744	18.02288884	0.348358703
Test 21	-0.00096	-1.59409	4951.617	21696.08	0.508769532	48.07617697	17.47208291	0.398003859
Test 22	0.399119	-1.59381	4949.603	21979.62	0.542051044	51.22111337	11.84207814	0.387643621
Test 23	0.798992	-1.59354	4946.916	19780.56	0.630384682	59.56820052	18.23230562	0.478365756
Test 24	1.198905	-1.59324	4954.304	21521.81	0.524216543	49.53584219	16.6318849	0.404694986
Test 25	1.598788	-1.59294	4940.2	23420.76	0.454597189	42.95716138	12.28023619	0.340757432
Avg			4948.447	22104.62	0.506137297	47.82744387	15.72482956	0.387751259
SD			6.959984	1359.467	0.07340015	6.935947165	2.142350223	0.050179155

Table-6.10 Indentation data for neat class-H cement (Used to get the maps in the results-Fig.4.10.)

Test	X	Y	Max Load	Max Depth	Hardness(GPa)	Hardness(HV)	Modulus	Martens
Test 1	0	-9.92E-06	4942.887	25568.16	0.351826	33.24582	15.77085	0.286078
Test 2	0.400101	0.000278	4956.318	23946.42	0.423065	39.97757	13.48138	0.327025
Test 4	1.199907	0.000804	4942.887	22412.19	0.475216	44.90551	16.45716	0.372319
Test 5	1.599809	0.001081	4959.005	28572.02	0.284297	26.86461	12.14605	0.229835
Test 6	-0.00023	-0.39858	4955.647	23576.76	0.428174	40.46028	15.33441	0.337314
Test 7	0.399863	-0.39826	4950.274	24271.3	0.408046	38.55833	13.62866	0.317941
Test 8	0.799806	-0.39796	4949.603	24335.03	0.421838	39.86158	11.39155	0.316235

Test 9	1.199728	-0.39761	4933.485	26080.52	0.337545	31.89628	15.10382	0.274425
Test 10	1.599601	-0.39727	4948.931	24706.19	0.392569	37.09584	13.33843	0.306763
Test 11	-0.00044	-0.79698	4948.259	22871.13	0.451846	42.6972	16.79072	0.357915
Test 12	0.399684	-0.79672	4956.318	23725.86	0.418581	39.55384	16.0431	0.333133
Test 13	0.799557	-0.79644	4949.603	25686.61	0.354775	33.52445	14.07167	0.283831
Test 14	1.1995	-0.79618	4945.573	25107.82	0.376681	35.59443	13.48929	0.296826
Test 15	1.599393	-0.79592	4950.274	27253.81	0.326608	30.86286	10.30492	0.252161
Test 16	-0.00066	-1.19564	4948.259	26608.4	0.352166	33.27789	9.570922	0.264434
Test 17	0.399427	-1.19537	4950.274	26313.73	0.340987	32.22155	12.7469	0.2705
Test 18	0.799309	-1.19508	4949.603	25296.23	0.376177	35.54683	12.43522	0.292659
Test 19	1.199222	-1.19484	4953.632	20605.76	0.560432	52.95798	20.13601	0.441417
Test 20	1.599125	-1.19457	4961.02	24542.29	0.385982	36.47334	16.39514	0.311633
Test 21	-0.00091	-1.59429	4959.005	24844.33	0.383748	36.26228	14.2272	0.303978
Test 22	0.399169	-1.59403	4952.289	26180.82	0.343129	32.42398	13.20834	0.273365
Test 23	0.799101	-1.59377	4937.514	24600.21	0.408314	38.58365	11.50979	0.308698
Test 24	1.199053	-1.59357	4938.186	20616.47	0.563997	53.29492	18.96616	0.439584

Test 25	1.598956	-1.59333	4956.318	27626.45	0.319971	30.23569	9.78742	0.245704
Test 26	1.998829	-1.59307	4945.573	24800.33	0.382316	36.12691	14.62066	0.304232
Avg			4949.629	24805.96	0.394731	37.30015	14.03823	0.30992
SD			6.831683	1871.575	0.065408	6.180766	2.575266	0.050549

Table-6.11 Indentation data for 5% Fer added class-H cement

Test	X	Y	Max Load	Max Depth	Hardness(GPa)	Hardness(HV)	Modulus	Martens
Test 1	1.98E-05	9.92E-06	4946.916	29959.7	0.262458	24.80093	9.886905	0.208527
Test 2	0.400141	0.000337	4952.289	29432.04	0.269857	25.50017	10.81534	0.216306
Test 3	0.800034	0.000585	4944.23	29070.43	0.281505	26.60083	9.912849	0.22136
Test 4	1.199976	0.000843	4954.304	27588.44	0.315465	29.80989	10.63041	0.246281
Test 5	1.599879	0.001131	4950.946	25789.12	0.364351	34.42936	11.59337	0.281655
Test 6	-0.00016	-0.39859	4952.289	27313.73	0.313782	29.65087	12.46956	0.251158
Test 7	0.399913	-0.39835	4951.617	28881.38	0.292523	27.64192	8.935291	0.224602
Test 8	0.799806	-0.39807	4952.961	28787.22	0.301852	28.52352	8.099122	0.226135
Test 9	1.199708	-0.39774	4934.828	28475.12	0.287022	27.12213	11.58676	0.230273
Test 10	1.599611	-0.39742	4955.647	24050.04	0.416723	39.37825	13.78459	0.324169
Test 11	-0.00043	-0.79709	4946.245	26826.19	0.332984	31.46528	11.25218	0.260052
Test 12	0.399665	-0.79684	4947.588	27018.17	0.318897	30.13418	13.10946	0.256439
Test 13	0.799538	-0.79659	4941.544	30427.87	0.305372	28.85614	4.991284	0.20194

Test 14	1.19943	-0.79637	4952.961	29435.53	0.273918	25.88389	9.90367	0.216284
Test 15	1.599313	-0.79612	4946.916	28001.24	0.301659	28.50531	11.07789	0.238717
Test 16	-0.00072	-1.19588	4952.961	28151.64	0.290601	27.46032	13.06588	0.236461
Test 17	0.399377	-1.19559	4956.99	26590.56	0.347391	32.82673	10.30717	0.265257
Test 18	0.7993	-1.19532	4934.828	25423.47	0.410329	38.77407	8.391664	0.288872
Test 19	1.199202	-1.19504	4951.617	24629.11	0.397422	37.55441	13.0613	0.308853
Test 20	1.599075	-1.19471	4938.857	26954.73	0.331873	31.36035	10.70552	0.257193
Test 21	-0.00096	-1.59443	4952.961	28458.19	0.286401	27.06345	12.18023	0.231395
Test 22	0.399159	-1.5941	4952.961	28574.28	0.29165	27.5595	10.32559	0.229518
Test 23	0.799042	-1.59383	4940.872	27043.07	0.318891	30.13359	12.80866	0.25562
Test 24	1.198944	-1.59356	4948.931	27608.89	0.303064	28.63805	13.22261	0.24565
Test 25	1.598867	-1.59334	4950.946	25080.88	0.381278	36.02889	12.90912	0.297787
Avg			4948.528	27582.84	0.319891	30.22808	11.00106	0.24882
SD			6.063661	1636.699	0.042703	4.035236	1.972779	0.030998

Table-6.12 Indentation data for 15% Fer added class-H cement

Test	X	Y	Max Load	Max Depth	Hardness(GPa)	Hardness(HV)	Modulus	Martens
Test 1	1.98E-05	9.92E-06	4959.005	26457.99	0.35169	33.23296	10.32896	0.26803
Test 2	0.400121	0.000278	4956.318	33363.84	0.214389	20.25867	7.498869	0.168465

Test 3	0.799994	0.000575	4954.975	28146	0.371527	35.10746	5.416141	0.236652
Test 4	1.199936	0.000863	4965.049	32814.5	0.214732	20.29112	9.506722	0.17446
Test 5	1.599859	0.001171	4942.215	32054.03	0.226326	21.38666	9.268718	0.181995
Test 6	-0.00017	-0.39851	4959.676	29954.97	0.265525	25.09074	9.442393	0.209131
Test 7	0.399942	-0.39824	4952.961	28288.95	0.29783	28.14346	10.48626	0.234171
Test 8	0.799796	-0.39794	4947.588	30376.23	0.256101	24.20026	9.454908	0.202875
Test 9	1.199718	-0.39766	4952.961	33539.91	0.204753	19.34811	9.163763	0.166588
Test 10	1.599631	-0.39739	4949.603	26484.74	0.374378	35.37683	8.0565	0.266982
Test 11	-0.00043	-0.79713	4956.318	28566.56	0.303292	28.65956	8.622766	0.229798
Test 12	0.399635	-0.79682	4949.603	28911.29	0.282928	26.73533	10.43029	0.224047
Test 13	0.799498	-0.79651	4957.662	33246.91	0.208666	19.71792	9.308094	0.169698
Test 14	1.19943	-0.7962	4950.274	34104.04	0.16564	15.65219	-20.7252	0.161035
Test 15	1.599363	-0.79592	4943.558	35612.07	0.180617	17.06739	8.315403	0.147485
Test 16	-0.00072	-1.19555	4958.333	29830.93	0.277402	26.21307	8.007853	0.210817
Test 17	0.399337	-1.19521	4951.617	30176.57	0.262894	24.8422	8.976567	0.205736
Test 18	0.79925	-1.19492	4947.588	27853.05	0.313355	29.61045	9.735799	0.241296
Test 19	1.199182	-1.19461	4948.931	33885.09	0.200238	18.92147	9.032346	0.163079

Test 20	1.599055	-1.19428	4944.901	33589.51	0.203778	19.25604	9.133318	0.165826
Test 21	-0.00105	-1.59397	4948.931	30379.58	0.257234	24.30731	9.22829	0.202885
Test 22	0.39904	-1.59366	4950.274	31896.84	0.230541	21.78501	8.980858	0.184093
Test 23	0.798932	-1.59335	4936.842	36150.77	0.176201	16.65015	7.691738	0.142928
Test 24	1.198835	-1.59299	4948.931	33361.43	0.204821	19.35456	9.918701	0.168238
Test 25	1.598698	-1.59266	4941.544	26123.72	0.350611	33.131	11.89372	0.273965
Avg			4951.026	31006.78	0.255819	24.1736	7.886953	0.200011
SD			6.374979	2861.646	0.06085	5.749979	5.961924	0.037868

Table-6.13 Indentation data for 30% Fer added class-H cement

6) Unconfined Compressive Strength data:

S. No	Sample	Diameter	Length	Axial load	UCS	UCS	UCS	Mass	Density	Aspect ratio	AVG
		in	in	Kn	psi	Kpsi	MPa	grams	grams/cc		
1	5% FERRIERITE	1.001	1.950	34.676	9,906	9.91	68.30	49.680	1.976	1.95	9934.06
2	5% FERRIERITE 2	1.001	1.948	35.499	10,141	10.14	69.92	49.767	1.981	1.95	
3	5% FERRIERITE 3	0.999	1.915	33.981	9,756	9.76	67.26	48.657	1.980	1.92	
4	15% FERRIERITE	0.991	1.950	22.857	6,662	6.66	45.93	48.436	1.965	1.97	6651.91
5	15% FERRIERITE 2	0.997	1.930	23.681	6,826	6.83	47.06	49.106	1.991	1.94	

6	15% FERRIERITE 3	0.991	1.919	22.169	6,468	6.47	44.59	47.702	1.969	1.94	
7	30% FERRIERITE	0.997	1.940	22.184	6,388	6.39	44.05	46.255	1.864	1.95	6319.00
8	30% FERRIERITE 2	1.001	1.960	22.039	6,296	6.30	43.41	46.936	1.857	1.96	
9	30% FERRIERITE 3	0.999	1.909	21.850	6,273	6.27	43.25	45.368	1.853	1.91	
10	NEAT CLASS H	1.198	1.984	35.623	7,111	7.11	49.03	74.111	2.024	1.66	7041.52
11	NEAT CLASS H 2	1.197	1.934	35.192	7,030	7.03	48.47	71.784	2.013	1.62	
12	NEAT CLASS H 3	1.199	1.973	35.045	6,984	6.98	48.15	73.769	2.022	1.65	

Table-6.14 UCS data for 16PPG Neat Class-H, 5%, 15%, and 30% ferrierite added class-H cement formulations

Glossary:

1. API – American Petroleum Institute
2. ASTM - American Society for Testing and Materials
3. NAS – National Academies of Sciences
4. GRP – Gulf Research Program
5. GoM – Gulf of Mexico
6. EIA – Energy Information Administration
7. BOEM – Beureau of Ocean Energy Management
8. SINTEF – Norwegian: Stiftelsen for industriell og teknisk forskning
9. NETL – National Energy Technology Laboratory
10. CEAT – College of Engineering, Architecture and technology

11. P&A – Plugging and abandonment
12. HPHT – High Pressure High Temperature
13. XRD – X-ray Diffraction
14. SEM – Scanning Electron microscopy
15. EDS – Energy Dispersive X-ray Spectroscopy
16. TEM – Transmission Electron Microscopy
17. XRF – X-ray Fluorescence.
18. UCS – Unconfined Compressive Strength
19. $Ca(OH)_2$ - Calcium hydroxide
20. NaCl – Sodium chloride (Table salt)
21. HCl – Hydrochloric Acid.
22. DI water – De-ionized water.
23. CH – Calium hydroxide (Cement terminology)
24. CSH – Calcium Silicate Hydrate (Cement terminology)
25. C_3A – Tricalcium aluminate (Cement terminology)
26. C_2S – Dicalcium silicate (Cement terminology)
27. Psi – Pounds per square inch.
28. GPa – Giga pascals.
29. µD – Micro Darcy.

VITA

Sai Vamsi Krishna Vissa

Candidate for the Degree of

Master of Science

Thesis: MICROSTRUCTURAL AND MECHANICAL CHARACTERIZATION OF ZEOLITE ENHANCED WELLBORE CEMENT FOR PLUGGING AND ABANDONMENT

Major Field: Petroleum Engineering

Biographical:

Education:

Completed the requirements for the Master of Science in Petroleum Engineering at Oklahoma State University, Stillwater, Oklahoma in December, 2021.

Completed the requirements for the Master of Science in Nanoscience and Nanotechnology at Sri Sathya Sai Institute of Higher Learning, Prasanthinilayam, Andhra Pradesh, India in 2016.

Completed the requirements for the Bachelor of Science in Biosciences (Honors) at Sri Sathya Sai Institute of Higher Learning, Bangalore, Karnataka, India in 2014.

Experience:

A total of 7 years of research experience including the masters and internships in India prior to arriving at Oklahoma State University. Expertise in Material synthesis and characterization, specialized in nanomaterials, semiconductors and hydraulic materials. Presented the work in several conferences and workshops Including AGU, SPE, and GRC, and published in the proceedings.

Professional Memberships:

FSAE (Formula SAE/Bullet racing) at OSU, SPE (Society of Petroleum Engineers) Oklahoma State Chapter.